

1 **Non-Hydrostatic RegCM4 (RegCM4-NH): Model description**  
2 **and case studies over multiple domains.**

3 Coppola [Erika](#) (1), Stocchi [Paolo](#) (2), Pichelli [Emanuela](#) (1), Torres [Alavez Jose Abraham](#)  
4 (1), Glazer [Russel](#) (1), Giuliani [Graziano](#) (1), Di Sante [Fabio](#) (1), Nogherotto [Rita](#) (1), Giorgi  
5 [Filippo](#) (1)

6  
7 *Correspondence to:* Erika Coppola ([coppolae@ictp.it](mailto:coppolae@ictp.it))

- 8 1. International Centre for Theoretical Physics (ICTP), Trieste, Italy  
9 2. Institute of Atmospheric Sciences and Climate, National Research Council of Italy, CNR-ISAC,  
10 Bologna, Italy

11 **Abstract**

12 We describe the development of a non-hydrostatic version of the regional climate model  
13 RegCM4, called RegCM4-NH, for use at convection-permitting resolutions. The non-  
14 hydrostatic dynamical core of the Mesoscale Model MM5 is introduced in the RegCM4,  
15 with some modifications to increase stability and applicability of the model to long-term  
16 climate simulations. Newly available explicit microphysics schemes are also described,  
17 and three case studies of intense convection events are carried out in order to illustrate  
18 the performance of the model. They are all run at convection-permitting grid spacing of 3  
19 km over domains in northern California, Texas and the Lake Victoria region, without the  
20 use of parameterized cumulus convection. A substantial improvement is found in [several](#)  
21 [aspects of](#) the simulations compared to corresponding coarser resolution (12 km) runs  
22 completed with the hydrostatic version of the model employing parameterized convection.  
23 RegCM4-NH is currently being used in different projects for regional climate simulations  
24 at convection-permitting resolutions, and is intended to be a resource for users of the  
25 RegCM modeling system.

26  
27 **Keywords:**

28 Regional climate models; RegCM4; km-scale resolution; climate change

29 **Introduction**

30 Since the pioneering work of Dickinson et al. (1989) and Giorgi and Bates (1989),  
31 [documenting the first regional climate modeling system \(RegCM, version 1\) in literature](#),  
32 the dynamical downscaling technique based on limited area Regional Climate Models

- Deleted: .
- Deleted: .
- Deleted: .
- Deleted: .
- Deleted: .
- Deleted: .
- Deleted: F.
- Deleted: R.
- Deleted: .

Deleted:

Formatted: Right: 0.63 cm

43 (RCMs) has been widely used worldwide, and a number of RCM systems have been  
 44 developed (Giorgi 2019). RegCM1 (Dickinson et al., 1989, Giorgi and Bates, 1989) was  
 45 originally developed at the National Center for Atmospheric Research (NCAR) based on  
 46 the Mesoscale Model version 4 (MM4) (Anthes et al, 1987). Then, further model versions  
 47 followed: RegCM2 (Giorgi et al. 1993a,b), RegCM2.5, (Giorgi and Mearns 1999),  
 48 RegCM3 (Pal et al. 2007), and lastly RegCM4 (Giorgi et al 2012). Except for the transition,  
 49 from RegCM1 to RegCM2, in which the model dynamical core was updated from that of  
 50 the MM4 to that of the MM5 (Grell et al. 1995), these model evolutions were mostly based  
 51 on additions of new and more advanced physics packages. RegCM4 is today used by a  
 52 large community for numerous projects and applications, from process studies to paleo  
 53 and future climate projections, including participation in the Coordinated Regional  
 54 Downscaling EXperiment (CORDEX, Giorgi et al. 2009; Gutowski et al. 2016). The model  
 55 can also be coupled with ocean, land and chemistry/aerosol modules in a fully interactive  
 56 way (Sitz et al. 2017).  
 57 The dynamical core of the standard version of RegCM4 is hydrostatic, with sigma-p  
 58 vertical coordinates. As a result, the model can be effectively run for grid spacings of ~10  
 59 km or larger, for which the hydrostatic assumption is valid. However, the RCM community  
 60 is rapidly moving to higher resolutions of a few km, i.e. "convection-permitting" (Prein et  
 61 al. 2015; Coppola et al. 2020) and therefore the dynamical core of RegCM4 has been  
 62 upgraded to include a non-hydrostatic dynamics representation usable for very high  
 63 resolution applications. This upgrade, which we name RegCM4-NH, is essentially based  
 64 on the implementation of the MM5 non-hydrostatic dynamical core within the RegCM4  
 65 framework, which has an entirely different set of model physics compared to MM5.  
 66  
 67 RegCM4-NH is already being used in some international projects focusing on climate  
 68 simulations at convection-permitting km-scales, namely the European Climate Prediction  
 69 System (EUCP, Hewitt and Lowe 2018) and the CORDEX Flagship Pilot Study dedicated  
 70 to convection (CORDEX-FPSCONV, Coppola et al. 2020), and it is starting to be used  
 71 more broadly by the RegCM modeling community.  
 72 For example, the recent papers by Ban et al. (2021) and Pichelli et al. (2021) document  
 73 results of the first multi-model experiment of 10-year simulations at the convection-  
 74 permitting scales over the so-called greater Alpine region. Two different simulations with  
 75 RegCM4-NH for present day conditions have contributed to the evaluation analysis of  
 76 Ban et al. (2021). They were carried out at the International Centre for Theoretical Physics  
 77 (ICTP) and the Croatian Meteorological and Hydrological Service (DHMZ) using two  
 78 different physics configurations. The results show that RegCM4-NH largely improves the  
 79 precipitation simulation as compared to available fine scale observations when going from  
 80 coarse to high resolution, in particular for higher order statistics, such as precipitation  
 81 extremes and hourly intensity, Pichelli et al. (2021) then analyse multi-model ensemble  
 82 simulations driven by selected CMIP5 GCM projections for the decades 1996–2005 and

**Deleted:** One of these systems, and in fact the first one to be developed, is the RegCM. The first version of RegCM, named ...egCM1 (Dickinson et al., 1989, and Bates, 1989), ... was (produced by Dickinson et al., (1989), and Giorgi and Bates, (1989) as a ...riginally developeddeveloped...at the National Center for Atmospheric Research (NCAR)ment...based onof...the Mesoscale Model version 4 (MM4) (Anthes et al, 1987) of the National Center for Atmospheric Research (NCAR)... Then, is was...followed by ...urther model versions followed: RegCM2 (Giorgi et al. 1993a,b), RegCM2.5, (Giorgi and Mearns 1999), RegCM3 (Pal et al. 2007), and lastly ... [1]

**Deleted:** passage...from RegCM1 to RegCM2, in which the model dynamical core was updated from that of the MM4 to that of the MM5 (Grell et al. 1995), these model evolutions were mostly based on additions of new and more advanced sub-grid...physics packages. In particular, ...egCM4 is today used by a large community for numerous projects and applications, from process studies to paleo and future climate projections, including participation into ... [2]

**Deleted:** more

**Deleted:** Long term simulations carried out through the new generation ...egCM4-NH is already being used incontribute to...some internationalbroad...projects focusing ondedicated to the study of...climate at the...convection-permitting km-scales,...namely the European Climate Prediction System (EUCP, Hewitt and Lowe 2018) and the CORDEX Flagship Pilot Study dedicated to convection (CORDEX-FPSCONV, Coppola et al. 2020), and it is starting to be used more broadly by the RegCM modeling community. ¶ ... [3]

**Deleted:** T...he recent papers by Ban et al. (2021) and Pichelli et al. (2021) document results of the first multi-model experiment of 10-year simulations at the convection-permitting scales over the so-called greater Aa...pine region. Two different simulations with RegCM4-NH for over the...present day conditions...have contributed to the evaluation analysis offer precipitation...(.an et al.,... (2021). They,...wererespectively...carried out atby the research group of...the International Centre for Theoretical Physics (ICTP) and the Croatian Meteorological and Hydrological Service (DHMZ) usingwith...two different physicscal... [4]

**Deleted:** EG

**Deleted:** simulations...largely improves reduce...the precipitation simulation asbias ... [5]

**Deleted:** with...available fine scale observations when going from coarse to higher ... [6]

**Deleted:** contributing to adding value to the representation of rainfall... Pichelli et al. (2021) then analyse the...multi-model ensemble simulations driven by selected CMIP5 GCM projections for theover [7]

**Formatted:** Right: 0.63 cm

187 2090–2099 under the RCP8.5 scenario. ICTP contributed to the experiment with  
188 simulations using RegCM4-NH, driven by the MOCH-HadGEM GCM (r1i1p1) in a two  
189 level nest configuration (respectively at 12 and 3 km grid). The paper shows new insights  
190 into future changes, for example an enhancement of summer and autumn hourly rainfall  
191 intensification compared to coarser resolution model experiments, as well as an increase  
192 of frequency and intensity of high-impact weather events.

- Deleted: rcp
- Deleted: performed by the new
- Deleted: core
- Deleted: with, among the others,
- Deleted: more than previously documented by
- Deleted: frequency

194 In this paper we describe the structure of RegCM4-NH and provide some illustrative  
195 examples of its performance, so that model users can have a basic reference providing  
196 them with background information on the model. In the next section we first describe the  
197 new model dynamical core, while the illustrative applications are presented in section 4.  
198 Section 5 finally provides some discussion of future developments planned for the RegCM  
199 system.

## 201 Model description

202 In the development of RegCM4-NH, the RegCM4 as described by Giorgi et al. (2012) was  
203 modified to include the non-hydrostatic dynamical core (*idynamic* = 2 namelist option as  
204 described in RegCM-4.7.1/Doc/README.namelist of the source code) of the mesoscale  
205 model MM5 (Grell et al. 1995). This dynamical core was selected because RegCM4  
206 already has the same grid and variable structure as MM5 in its hydrostatic core, which  
207 substantially facilitated its implementation (Elguindi et al. 2017).

- Deleted: as an additional option selectable through a switch,...
- Deleted: , which uses the equations described by Grell et al. (1995)...
- Deleted: shares with it
- Deleted: it
- Deleted: follows
- Deleted: for
- Deleted: of the RegCM4
- Deleted: standard

209 The model equations with complete description of the Coriolis force and a top radiative  
210 boundary condition, along with the finite differencing scheme, are given in Grell et al.  
211 (1995). Pressure,  $p$ , temperature,  $T$ , and density,  $\rho$ , are first decomposed into a  
212 prescribed reference vertical profile plus a time varying perturbation. The prognostic  
213 equations are then calculated using the pressure perturbation values. Compared to the  
214 original MM5 dynamical core, the following modifications were implemented in order to  
215 achieve increased stability for long term climate simulations (Elguindi et al. 2017  
216 document any modifications which follow the choice of the non-hydrostatic dynamical  
217 core through the namelist parameter *idynamic* = 2; further available user-dependant  
218 options, and the corresponding section in the namelist, are explicitly indicated):

219  
220 i) The reference state temperature profile is computed using a latitude dependent  
221 climatological temperature distribution and thus is a function of the specific domain  
222 coordinates (*base\_state\_pressure*, *logp\_lrate* parameters in *&referenceatm*) (Elguindi et  
223 al. 2017). These two parameters were hard-coded in the original MM5 while for the  
224 RegCM are user configurable;

- Deleted: surface
- Commented [1]: added the configurability comment here-
- Formatted: Right: 0.63 cm

243 ii) The lateral time dependent boundary conditions (*iboudy* in *&physicsparam*) for each  
 244 prognostic variable use the same exponential relaxation technique (*iboudy* = 5) described  
 245 in Giorgi et al. (1993). The linear MM5 relaxation scheme is [also](#) kept as an option (*iboudy*  
 246 = 1);

Deleted: only

247  
 248 iii) The advection term in the model equations, which in the MM5 code is implemented  
 249 using a centered finite difference approach, was changed to include a greater upstream  
 250 weight factor as a function of the local Courant number (Elguindi et al. 2017). The  
 251 maximum value of the weight factor is user configurable (*uoffc* in *&dynparam*). As detailed  
 252 in the MM5 model description (Grell et al, 1995), the horizontal advection term for a scalar  
 253 variable X contributes to the total tendency as:

$$\Delta_{adv}(p^*X)_G = -m^2|_G \left[ \frac{(p^*X|_{b\frac{u}{m}}|_b - p^*X|_{a\frac{u}{m}}|_a)}{dx} + \frac{(p^*X|_{d\frac{v}{m}}|_d - p^*X|_{c\frac{v}{m}}|_c)}{dy} \right]$$

255  
 256 where the *m* is the projection mapping factor and, with respect to Figure 1, assuming that  
 257 the computation is to be performed for the gold cross point *G*, the averages are performed  
 258 in the points *a, b, c, d*. For the *u/m* and *v/m* terms, the average value is computed using  
 259 respectively the values in points *AC, BD, CD, AB*.

Commented [2]: Added the equation description-

260 In RegCM4 for the term *p^\*X*, the model computes a weighted average value of the field  
 262 using the value in gold+cyan and gold+green cross points with weights increasing the  
 263 relative contribution of the upstream point up as a function of the local courant number:

$$\begin{aligned} 264 \quad p^*X|_a &= 0.5((1 - f_1)p^*X|_G + (1 + f_1)p^*X|_{c_1}) \\ 265 \quad p^*X|_b &= 0.5((1 - f_1)p^*X|_{c_2} + (1 + f_1)p^*X|_G) \\ 266 \quad p^*X|_c &= 0.5((1 - f_2)p^*X|_G + (1 + f_2)p^*X|_{g_1}) \\ 267 \quad p^*X|_d &= 0.5((1 - f_2)p^*X|_{g_2} + (1 + f_2)p^*X|_G) \end{aligned}$$

268 where *f<sub>1</sub>*, *f<sub>2</sub>* are defined as the local Courant number for the 1D advection equations  
 269 multiplied for a control factor:

$$\begin{aligned} 270 \quad f_1 &= \mu_{fc}dt \frac{(u|_a + u|_b)}{2dx} \\ 271 \quad f_2 &= \mu_{fc}dt \frac{(v|_c + v|_d)}{2dy} ; \end{aligned}$$

Commented [3]: Added equation description

274

Formatted: Right: 0.63 cm

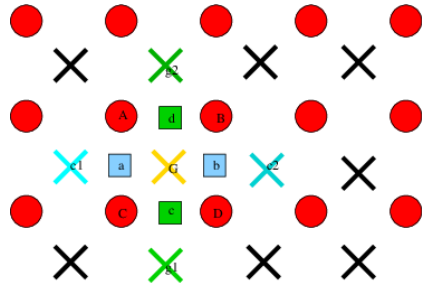


**Figure 1 Schematic representation showing the horizontal advection scheme staggering. Circles are U,V points. X are scalar variable points.**

276  
277  
278  
279  
280  
281  
282  
283  
284  
285  
286  
287  
288  
289  
290  
291  
292  
293  
294  
295  
296  
297  
298  
299  
300  
301  
302  
303  
304  
305

iv) The water species (cloud, ice, rain, snow) term uses the same advection scheme as the other variables (Elguindi et al. 2017) and not a complete upstream scheme as in the MM5 code (Grell et al. 1995);

Deleted: moisture

v) A local flux limiter reduces the advection terms in order to remove unrealistic strong gradients and its limits are user configurable (in the &dynparam section the maximum gradient fraction for advection; temperature, t\_extrema, specific humidity, q\_rel\_extrema, liquid cloud content, c\_rel\_extrema and for tracers, t\_rel\_extrema). This was hardcoded in the MM5 code and the limits were not user configurable;

Deleted: to stop for

vi) The diffusion stencil of the Laplace equation uses a nine point approach as in LeVeque (2006) and a topography dependent environmental diffusion coefficient is added to reduce spurious diffusion along pressure coordinate slopes (Elguindi et al. 2017) as in the hydrostatic version of the code (Giorgi et al. 1993b). The change in stencil does not affect the overall fourth order precision of the model, but reduces the computational stencil size, thus reducing the communication overhead;

Deleted: used

vii) The top boundary radiative condition (ifupr = 1 in &nonhydroparam) adopted in the semi-implicit vertical differencing scheme to reduce the reflection of energy waves uses coefficients on a 13x13 matrix which are re-computed every simulation day and not kept constant throughout the whole simulation as in the MM5 code. This allows the model to be run for longer simulation times while not being strongly tied to the initial atmospheric conditions;

Formatted: Right: 0.63 cm

309 viii) The dynamical control parameter  $\beta$  in the semi-implicit vertical differencing scheme  
 310 (*nhbet* in *&nonhydroparam*) used for acoustic wave damping (Elguindi et al. 2017) is user  
 311 configurable (Klemp and Dudhia, 2008), while it is hard-coded in the MM5;

Deleted: is  
 Deleted: and  
 Deleted: code

312  
 313 ix) A Rayleigh damping (*ifrayd* = 1 in *&nonhydroparam*) of the status variables towards  
 314 the input GCM boundary conditions can be activated in the top layers (*rayndamp*  
 315 configuring the number of top levels to apply) with a configurable relaxation time  
 316 (*rayalpha0*, Klemp and Lilly, 1978, Durran and Klemp, 1983. This is consistent to what is  
 317 implemented in the WRF model);

318  
 319 x) The water species time filtering uses the Williams (2009) modified filter with  $\alpha = 0.53$   
 320 instead of the RA filter used by all the other variables. The  $v$  factor in the RA filter is user  
 321 configurable (*gnu1* and *gnu2* in *&dynparam*). This reduces the damping introduced by the  
 322 Robert-Asselin filter and the computational diffusion introduced by the horizontal  
 323 advection scheme.

324  
 325 With these modifications, the model basic equations, under leap-frog integration scheme,  
 326 are, (Elguindi et al. 2017) :

Deleted: the (same as in the MM5) and namely  
 Deleted: are

327  
 328  
 329 
$$\frac{\partial p^* u}{\partial t} = -m^2 \left[ \frac{\partial p^* u u / m}{\partial x} + \frac{\partial p^* v u / m}{\partial y} \right] - \frac{\partial p^* u \dot{\sigma}}{\partial \sigma} + u DIV -$$

$$\frac{m p^*}{\rho} \left[ \frac{\partial p'}{\partial x} - \frac{\sigma}{p^*} \frac{\partial p^*}{\partial x} \frac{\partial p'}{\partial \sigma} \right] + p^* f v - p^* e w \cos \theta + D_u \quad (1)$$
 330

331 
$$\frac{\partial p^* v}{\partial t} = -m^2 \left[ \frac{\partial p^* u v / m}{\partial x} + \frac{\partial p^* v v / m}{\partial y} \right] - \frac{\partial p^* v \dot{\sigma}}{\partial \sigma} + v DIV -$$

$$\frac{m p^*}{\rho} \left[ \frac{\partial p'}{\partial y} - \frac{\sigma}{p^*} \frac{\partial p^*}{\partial y} \frac{\partial p'}{\partial \sigma} \right] - p^* f u + p^* e w \sin \theta + D_v \quad (2)$$
 332

333 
$$\frac{\partial p^* w}{\partial t} = -m^2 \left[ \frac{\partial p^* u w / m}{\partial x} + \frac{\partial p^* v w / m}{\partial y} \right] - \frac{\partial p^* w \dot{\sigma}}{\partial \sigma} + w DIV +$$

$$p^* g \frac{\rho_0}{\rho} \left[ \frac{1}{p^*} \frac{\partial p'}{\partial \sigma} + \frac{T'_v}{T} - \frac{T_0 p'}{T p_0} \right] - p^* g [(q_c + q_r)] + p^* e (u \cos \theta - v \sin \theta) + D_w \quad (3)$$
 334

335 
$$\frac{\partial p^* p'}{\partial t} = -m^2 \left[ \frac{\partial p^* u p' / m}{\partial x} + \frac{\partial p^* v p' / m}{\partial y} \right] - \frac{\partial p^* p' \dot{\sigma}}{\partial \sigma} + p' DIV -$$

$$m^2 p^* \gamma p \left[ \frac{\partial u / m}{\partial x} - \frac{\sigma}{m p^*} \frac{\partial p^*}{\partial x} \frac{\partial u}{\partial \sigma} + \frac{\partial v / m}{\partial y} - \frac{\sigma}{m p^*} \frac{\partial p^*}{\partial y} \frac{\partial v}{\partial \sigma} \right] + \rho_0 g \gamma p \frac{\partial w}{\partial \sigma} + p^* \rho_0 g \quad (4)$$

Formatted: Right: 0.63 cm

341

$$\frac{\partial p^* T}{\partial t} = -m^2 \left[ \frac{\partial p^* u T/m}{\partial x} + \frac{\partial p^* v T/m}{\partial y} \right] - \frac{\partial p^* T \dot{\sigma}}{\partial \sigma} + T DIV + \frac{1}{\rho c_p} \left[ p^* \frac{Dp'}{Dt} - \rho_0 g p^* w - D_{p'} \right] + p^* \frac{\dot{Q}}{c_p} + D_T \quad (5)$$

342

343

344

Where:

345

$$DIV = m^2 \left[ \frac{\partial p^* u/m}{\partial x} + \frac{\partial p^* v/m}{\partial y} \right] + \frac{\partial p^* \dot{\sigma}}{\partial \sigma}$$

346

$$\dot{\sigma} = -\frac{\rho_0 g}{p^*} w - \frac{m \sigma}{p^*} \frac{\partial p^*}{\partial x} u - \frac{m \sigma}{p^*} \frac{\partial p^*}{\partial y} v$$

347

$$\tan \theta = -\cos \phi \frac{\partial \lambda / \partial y}{\partial \phi / \partial x}$$

348

$$p(x, y, z, t) = p_0(z) + p'(x, y, z, t)$$

349

$$T(x, y, z, t) = T_0(z) + T'(x, y, z, t)$$

350

$$\rho(x, y, z, t) = \rho_0(z) + \rho'(x, y, z, t)$$

351

with the vertical sigma coordinate, defined as:

352

$$\sigma = \frac{(p_0 - p_t)}{(p_s - p_t)}$$

353

354

where  $p_s$  is the surface pressure and  $p_0$  is the reference pressure profile. The total pressure

355

at each grid point is thus given as:

356

357

$$p(x, y, z, t) = p^* \sigma(k) + p_t + p'(x, y, z, t)$$

358

359

360

With  $p_t$  being the top model pressure assuming a fixed rigid lid.

Deleted: and

Deleted: is

Formatted: Right: 0.63 cm

363 The model physics schemes for boundary layer, radiative transfer, land and ocean  
 364 surface processes, cloud and precipitation processes are extensively described in Giorgi  
 365 et al. (2012) and summarized in Table 1. For each physics component a number of  
 366 parameterization options are available (Table 1), and can be selected using a switch  
 367 selected by the user. As mentioned, the use of non-hydrostatic dynamics is especially  
 368 important when going to convection-permitting resolutions of a few km (Prein et al. 2015).  
 369 At these resolutions the scale separation assumption underlying the use of cumulus  
 370 convection schemes is not valid any more, and explicit cloud microphysics  
 371 representations are necessary. The RegCM4 currently includes two newly implemented  
 372 microphysics schemes, the Nogherotto-Tompkins (Nogherotto et al. 2016) and the WSM5  
 373 scheme from the Weather Research Forecast (WRF, Skamarok et al. 2008) model, which  
 374 are briefly described in the next sections for information to model users.

375

<u>Model physics (Namelist flag)</u>	<u>Options</u>	<u>n. option</u>	<u>Reference</u>
<u>Dynamical core (idynamic)</u>	<u>Hydrostatic</u>	<u>1</u>	<u>Giorgi et al. 1993a,b</u> <u>Giorgi et al. 2012</u>
	<u>Non-Hydrostatic (*)</u>	<u>2</u>	<u>present paper</u>
<u>Radiation (irrtm)</u>	<u>CCSM</u>	<u>0</u>	<u>Kiehl et al. 1996</u>
	<u>RRTM (*)</u>	<u>1</u>	<u>Mlawer et al. 1997</u>
<u>Microphysics (ipptls)</u>	<u>Subex</u>	<u>1</u>	<u>Pal et al 2000</u>
	<u>Nogherotto Thompkins</u>	<u>2</u>	<u>Nogherotto et al. 2016</u>
	<u>WSM5 (*)</u>	<u>3</u>	<u>Hong et al 2004</u>
<u>Cumulus (icup)</u>	<u>Kuo</u>	<u>1</u>	<u>Anthes et al. 1987</u>
	<u>Grell</u>	<u>2</u>	<u>Grell 1993</u>
	<u>Emanuel</u>	<u>4</u>	<u>Emanuel 1991</u>
	<u>Tiedtke</u>	<u>5</u>	<u>Tiedtke 1989, 1993</u>

Deleted: resumed

Deleted: references therein

Deleted: model

Formatted: Right: 0.63 cm



	<u>Kain-Fritsch</u>	<u>6</u>	<u>Kain and Fritsch, 1990; Kain 2004</u>
	<u>MM5 Shallow cumulus (only mixing) (*)</u>	<u>-1</u>	<u>Grell et al. 1994</u>
<u>Planetary Boundary Layer (ibltyp)</u>	<u>Modified-Holtslag</u>	<u>1</u>	<u>Holtslag et al., 1990</u>
	<u>UW</u>	<u>2</u>	<u>Bretherton et al. 2004</u>
<u>Land Surface (code compiling option)</u>	<u>BATS</u>	<u>1</u>	<u>Dickinson et al. 1993; Giorgi et al. 2003</u>
	<u>CLM4.5</u>	<u>1</u>	<u>Oleson et al. 2013</u>
<u>Ocean Fluxes (iocnflx)</u>	<u>BATS</u>	<u>1</u>	<u>Dickinson et al. 1993</u>
	<u>Zeng</u>	<u>2</u>	<u>Zeng et al. 1998</u>
	<u>COARE</u>	<u>3</u>	<u>Fairall et al. 1996a,b</u>
<u>Interactive lake (lakemod)</u>	<u>1D diffusion/convection</u>	<u>1</u>	<u>Hostetler et al. 1993</u>
<u>Tropical band (i_band)</u>	<u>RegT-Band</u>	<u>1</u>	<u>Coppola et al. 2012</u>
<u>Coupled ocean (iocncpl)</u>	<u>RegCM-ES</u>	<u>1</u>	<u>Sitz et al. 2017</u>

**Table 1 Core and sub-grid physics scheme available in RegCM-NH. New schemes available with this release are starred (\*).**

**Explicit microphysics schemes:**

379  
380  
381  
382  
383  
384

Formatted: Font: 12 pt, Font colour: Auto

Formatted: Normal

Formatted: Right: 0.63 cm

385 *Nogherotto-Tompkins Scheme:*

386 A new parameterization for explicit cloud microphysics and precipitation built upon the  
387 European Centre for Medium Weather Forecast's Integrated Forecast System (IFS)  
388 module (Tiedtke, 1993, Tompkins, 2007), was introduced in RegCM4 (*ipptls* = 2 in  
389 *&microparam*) by Nogherotto et al. (2016). In the present configuration, the scheme  
390 implicitly solves 5 prognostic equations for water vapor, *qv*, cloud liquid water, *ql*, rain, *qr*,  
391 cloud ice, *qi*, and snow, *qs*, but it is also easily extendable to a larger number of variables.  
392 Water vapor, cloud liquid water, rain, cloud ice and snow are all expressed in terms of the  
393 grid-mean mixing ratio.

394 Cloud liquid and ice water content are independent, allowing the existence of supercooled  
395 liquid water and mixed-phase clouds. Rain and snow precipitate with a fixed terminal fall  
396 speed and can then be advected by the three dimensional winds. A check for the  
397 conservation of enthalpy and of total moisture is ensured at the end of each timestep. The  
398 governing equation for each variable is:  
399

$$\frac{\partial q_x}{\partial t} = S_x + \frac{1}{\rho} \frac{\partial}{\partial z} (\rho V_x q_x)$$

400  
401

402 The local variation of the mixing ratio *qx* of the variable *x* is given by the sum of *Sx*,  
403 containing the net sources and sinks of *qx* through microphysical processes (i.e.  
404 condensation, evaporation, auto-conversion, melting, etc.), and the sedimentation term,  
405 which is a function of the fall speed *Vx*. An upstream approach is employed to solve the  
406 equations. The sources and sinks contributors are divided in two groups according to the  
407 duration of the process they describe: processes that are considered to be fast relative to  
408 the model time step are treated implicitly while slow processes are treated explicitly. The  
409 processes taken into account (shown in Figure 2) are the microphysical pathways across  
410 the 5 water variables: condensation, autoconversion, evaporation, cloud water collection  
411 (accretion), and autoconversion for warm clouds, and freezing, melting, deposition,  
412 sublimation for cold clouds.

413

Deleted: solves implicitly

Deleted: qv

Deleted: ql

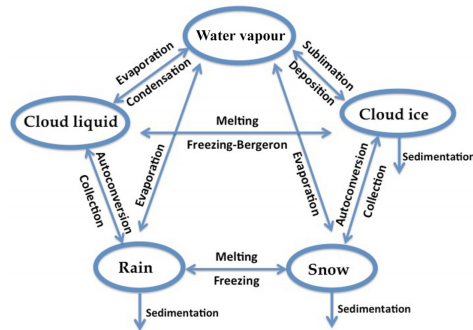
Deleted: qr

Deleted: qi

Deleted: qs

Deleted: 1

Formatted: Right: 0.63 cm



421

422 **Figure 2: Depiction of the new scheme, showing the five prognostic variables and**  
 423 **how they are related to each other through microphysical processes**

Deleted: 1

424 For each microphysical pathway, phase changes are associated with the release or  
 425 absorption of latent heat, which then impacts the temperature budget. The impact is  
 426 calculated using the conservation of liquid water temperature  $T_L$  defined as:  
 427

428 
$$T_L = T - \frac{L_v}{C_p}(q_l + q_r) - \frac{L_s}{C_p}(q_i + q_s).$$

429 Given that  $dT_L = 0$ , the rate of change of the temperature is given by the following  
 430 equation:

431

432 
$$\frac{\partial T}{\partial t} = \sum_{x=1}^m \frac{L(x)}{C_p} \left( \frac{dq_x}{dt} - D_{q_x} - \frac{1}{\rho} \frac{\partial}{\partial z} (\rho V_x q_x) \right)$$

433

434 where  $L(x)$  is the latent heat of fusion or evaporation, depending on the process  
 435 considered,  $D_{q_x}$  is the convective detrainment and the third term in brackets is the  
 436 sedimentation term.

437 At the end of each time step a check is carried out of the conservation of total water and  
 438 moist static energy:  $h = C_p T + gz + Lq_x.$

439 The scheme is tunable through parameters in the *&microparam* section of the namelist  
 440 (RegCM-4.7.1/Doc/README.namelist; Elguindi et al. 2017).

Formatted: Right: 0.63 cm

442 *WSM5 Scheme:*

443 RegCM4-NH also employs the Single-Moment 5-class microphysics scheme of the WRF  
444 model (Skamarock et al., 2008). This scheme (*ipptls* = 3 in *&microparam*) follows Hong  
445 et al. (2004) and, similarly to Nogherotto et al. (2016), includes vapor, rain, snow, cloud  
446 ice, and cloud water hydrometeors. The scheme separately treats ice and water  
447 saturation processes, assuming water hydrometeors for temperatures above freezing,  
448 and cloud ice and snow below the freezing level (Dudhia, 1989, Hong et al., 1998). It  
449 accounts for supercooled water and a gradual melting of snow below the melting layer  
450 (Hong et al., 2004, and Hong and Lim, 2006). Therefore, the WSM5 and Nogherotto-  
451 Tompkins schemes have similar structures (Figure 2), but also important differences.

Deleted: 1

452 Differently from the Nogherotto-Tompkins scheme, the WSM5 (as well as the other WSM  
453 schemes in WRF) prescribes an inverse exponential continuous distribution of particle  
454 size (ex. Marshall and Palmer (1948) for rain, Gunn and Marshall (1958) for snow). It also  
455 includes the size distribution of ice particles and, as a major novelty, the definition of the  
456 number of ice crystals based on ice mass content rather than temperature. Both the  
457 Nogherotto-Tompkins and WSM5 schemes include autoconversion, i.e. sub-time step  
458 processes of conversion of cloud water to rain and cloud ice to snow. For rain, Hong et  
459 al. (2004) use a Kessler (1969) type algorithm in WSM5, but with a stronger physical basis  
460 following Tripoli and Cotton (1980). The Nogherotto-Tompkins scheme also includes the  
461 original Kessler (1969) formula as an option, but it makes available other three  
462 exponential approaches following Sundqvist et al. (1989), Beheng (1994), and  
463 Khairoutdinov and Kogan (2000). For ice autoconversion the Nogherotto-Tompkins  
464 scheme uses an exponential approach (Sundqvist, 1989) with a specific coefficient for ice  
465 particles (following Lin et al., 1983) depending on temperature, while the WSM5 uses a  
466 critical value of ice mixing ratio (depending on air density) and a maximum allowed ice  
467 crystal mass (following Rutledge and Hobbs, 1983) that suppresses the process at low  
468 temperatures because of the effect of air density. Finally, the WSM5 has no dependency  
469 on cloud cover for condensation processes while the Nogherotto-Tompkins scheme uses  
470 cloud cover to regulate the condensation rate in the formation of stratiform clouds.

471

## 472 **Illustrative case studies**

473

474 Three case studies (Table 2) of Heavy Precipitation Events (HPE) have been identified in  
475 order to test and illustrate the behavior of the non-hydrostatic core of the RegCM4-NH,  
476 with focus on the explicit simulation of convection over different regions of the world. In  
477 two test cases, California and Lake Victoria, data from the ERA-Interim reanalysis (Dee

Deleted: 1

Formatted: Right: 0.63 cm

480 et al. 2011) are used to provide initial and lateral meteorological boundary conditions for  
481 an intermediate resolution run (grid spacing of 12 km, with use of convection  
482 parameterizations) (Figure 3), which then provides driving boundary conditions for the  
483 convection-permitting experiments. In the Texas case study, however, we nested the  
484 model directly in the ERA-Interim reanalysis with boundary conditions provided every 6  
485 hours, given that such configuration was able to reproduce accurately the HPE intensity.  
486 In this case the model uses a large LBC relaxation zone which allows the description of  
487 realistic fine-scale features driving this weather event (even if not fully consistent with the  
488 Matte et al. (2017) criteria). All simulations start 24-48 hours before the HPE. The analysis  
489 focuses on the total accumulated precipitation over the entire model domain at 3 km  
490 resolution (Fig. 3) for the periods defined in Table 2. In the cases of California and Texas  
491 the evaluation also includes the time series of 6 hourly accumulated precipitation  
492 averaged on the region of maximum precipitation (black rectangles in Figs. 3) against  
493 available high temporal resolution observations (NCEP/CPC) (Table 3). The discussion  
494 of the case studies is presented in the next sections; the configuration files (namelists)  
495 with full settings for the three test cases are available at  
496 <https://zenodo.org/record/5106399>.

498 A key issue concerning the use of CP-RCMs is the availability of very high resolution,  
499 high quality observed datasets for the assessment and evaluation of the models, which  
500 is not there for most of the world regions. Precipitation measurements come from  
501 essentially three distinct sources: in-situ rain-gauges, ground radar and satellite. In the  
502 present study we use 7 observational datasets depending on the case study and the area  
503 covered, as described in Table 2. We have used: Precipitation Estimation from Remotely  
504 Sensed Information using Artificial Neural Networks - Climate Data Record (PERSIAN-  
505 CDR), Climate Hazards Group InfraRed Precipitation with Station data (CHIRPS), the  
506 Climate Prediction Center morphing method (CMORPH), Tropical Rainfall Measuring  
507 Mission (TRMM), NCEP/CPC-Four Kilometer Precipitation Set Gauge and Radar  
508 (NCEP/CPC), CPC-Unified daily gauge based precipitation estimates (CPC) and  
509 Parameter-elevation Regressions on Independent Slopes Model (PRISM) (Table 3).  
510 NCEP/CPC is a precipitation analysis which merges a rain gauge dataset with radar  
511 estimates. CMORPH and PERSIAN-CDR are based on satellite measurements, CHIRPS  
512 incorporates satellite imagery with in-situ station data. CPC is a gauge-based analysis of  
513 daily precipitation and the PRISM dataset gathers climate observations from a wide range

Deleted: 2

Deleted:

Deleted: In the Texas case study, we fed directly the fields from the ERA-Interim reanalysis to the RegCM 3km convection permitting simulation, because we found that the HPE intensity was already reproduced accurately with this procedure

Deleted: domains

Deleted: of

Deleted: 2

Deleted: and

Deleted: 1

Deleted: For

Deleted: 4

Deleted: ab

Formatted: Right: 0.63 cm

529 of monitoring networks, applies sophisticated quality control measures, and develops  
 530 spatial climate datasets incorporating a variety of modeling techniques at multiple spatial  
 531 and temporal resolutions.

532

533

<u>Case</u>	<u>ACRONYM</u>	<u>Region of The event</u>	<u>Domains size lon x lat x vertical levels</u>	<u>Simulation Time Window</u>
<u>1</u>	<u>CAL</u>	<u>California</u>	<u>480 x 440 x 41</u>	<u>15 Feb 2004 00:00</u> <u>19 Feb 2004 00:00</u>
<u>2</u>	<u>TEX</u>	<u>Texas</u>	<u>480 x 440 x 41</u>	<u>9 June 2010 00:00</u> <u>12 June 2010 00:00</u>
<u>3</u>	<u>LKV</u>	<u>Lake Victoria</u>	<u>550 x 530 x 41</u>	<u>25 Nov 1999 00:00</u> <u>1 Dec 1999 00:00</u>

534 **Table 2: List of acronyms and description of the test cases with corresponding 3km**  
 535 **domain sizes and simulation period.**

Deleted: and

536

<u>Dataset name</u>	<u>Region</u>	<u>Spatial Resolution</u>	<u>Temporal Resolution</u>	<u>Data Source</u>	<u>Reference</u>
<u>TRMM</u>	<u>World</u>	<u>0.5°</u>	<u>Daily</u>	<u>Satellite</u>	<u>Huffman et al. (2007)</u>
<u>CHIRPS</u>	<u>World</u>	<u>0.05°</u>	<u>Daily</u>	<u>Station data+Satellite</u>	<u>Funk et al. (2015)</u>
<u>CMORPH</u>	<u>World</u>	<u>0.25°</u>	<u>Daily</u>	<u>Satellite</u>	<u>Joyce et al.</u>

Formatted: Right: 0.63 cm

					(2004)
<a href="#">NCEP/CPC</a>	<a href="#">USA</a>	<a href="#">0.04°</a>	<a href="#">Hourly</a>	<a href="#">Gauge and Radar</a>	<a href="https://doi.org/10.5065/D69Z93M3">https://doi.org/10.5065/D69Z93M3</a> . Accessed: 27/06/2018
<a href="#">CPC</a>	<a href="#">World</a>	<a href="#">0.5°</a>	<a href="#">Daily</a>	<a href="#">Station data</a>	<a href="#">Chen and Xie (2008)</a>
<a href="#">PRISM</a>	<a href="#">USA</a>	<a href="#">0.04°</a>	<a href="#">Daily</a>	<a href="#">Station data</a>	<a href="#">PRISM Climate Group. 2016.</a>
<a href="#">PERSIAN-CDR</a>	<a href="#">World</a>	<a href="#">0.25°</a>	<a href="#">Daily</a>	<a href="#">Satellite</a>	<a href="#">Ashouri et al. (2015)</a>

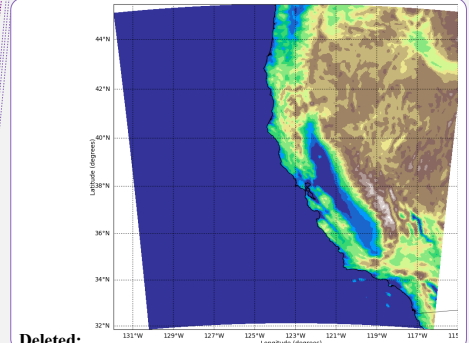
Table 3: List of **observed precipitation datasets** used for comparison.

▼	▼
▼	▼
▼	▼
▼	▼

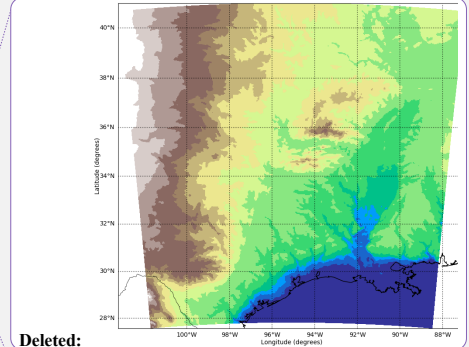
Deleted: gridded

Deleted: CAL (a)

Deleted: TEX (b)

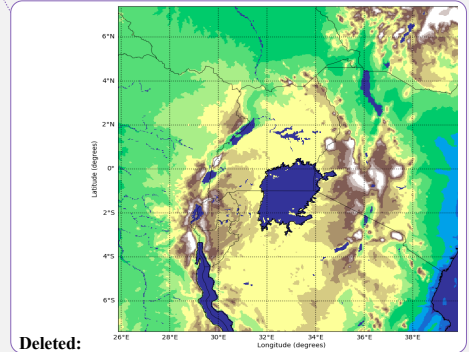


Deleted:



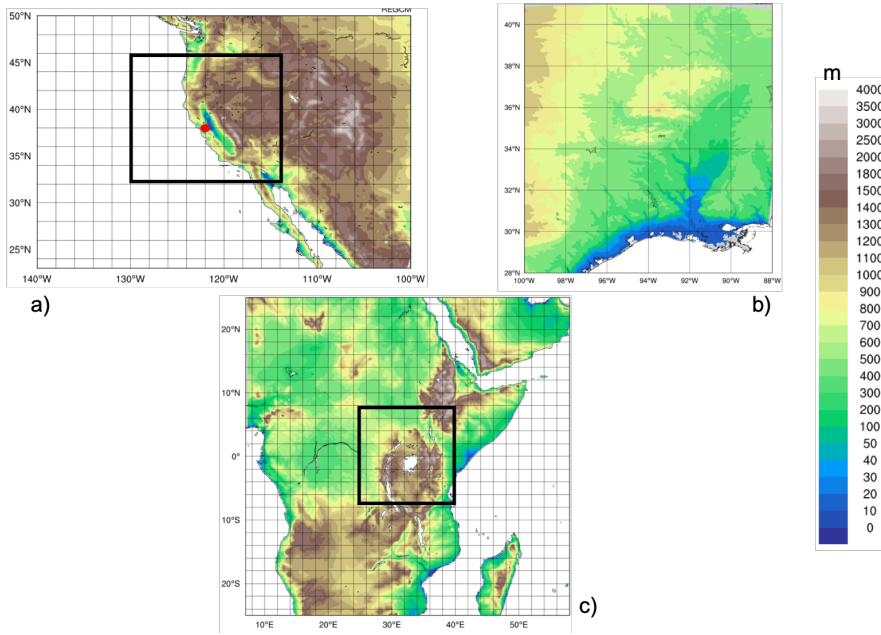
Deleted:

Deleted: LKV (c)



Deleted:

Formatted: Right: 0.63 cm



547

548 **Figure 3: Simulation domains tested , a) California (CAL) , b) Texas (TEX), c) Lake**  
 549 **Victoria (LKV) . For CAL (a) and LKV (b) the black square shows the 3 km simulation**  
 550 **domains nested in the 12 km domain in figure. For TEX the 3 km domain simulation**  
 551 **(c) is fed directly with the ERA-Interim reanalysis fields.**

552

553

554 **California**

555 The first case, referred to as CAL (California) in Table 2, is a HPE which occurred on 16–  
 556 18 February 2004, producing flooding conditions for the Russian River, a southward-  
 557 flowing river in the Sonoma and Mendocino counties of northern California (red-dot)  
 558 (Figure 3). The event is documented in detail by Ralph et al. (2006), who focused their

Deleted: 2  
 Deleted: D

Deleted: 1

Deleted: in coastal

Deleted: f

Deleted: 2

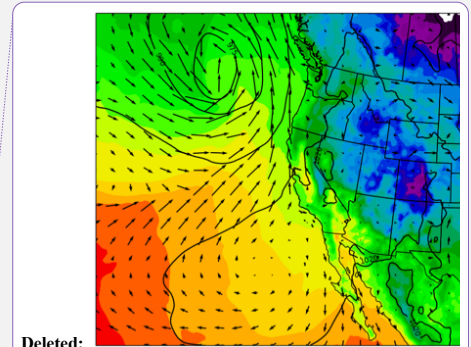
Formatted: Right: 0.63 cm



565 attention on the impact of narrow filament-shaped structures of strong horizontal water  
566 vapor transport over the eastern Pacific Ocean and the western U.S. coast, called  
567 Atmospheric Rivers (ARs). ARs are typically associated with a low-level jet stream ahead  
568 of the cold front of extratropical cyclones (Zhu and Newell 1998; Dacre et al. 2015; Ralph  
569 et al. 2018), and can induce heavy precipitation where they make landfall and are forced  
570 to rise over mountain chains (Gimeno et al. 2014). The CAL event consists of a slow  
571 propagating surface front arching southeastward towards Oregon and then  
572 southwestward offshore of California (Fig.3a,c). Rain began over the coastal mountains  
573 of the Russian River watershed at 0700 UTC, 16 February, as a warm front descended  
574 southward, and also coincided with the development of orographically favoured low-level  
575 upslope flow Ralph et al. (2006).

576

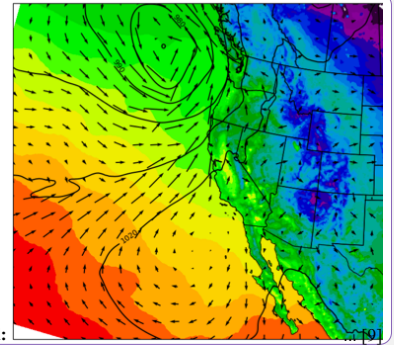
▼	▼
▼	▼



Deleted:

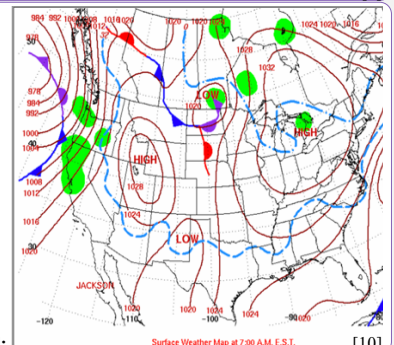
a)

[8]



Deleted:

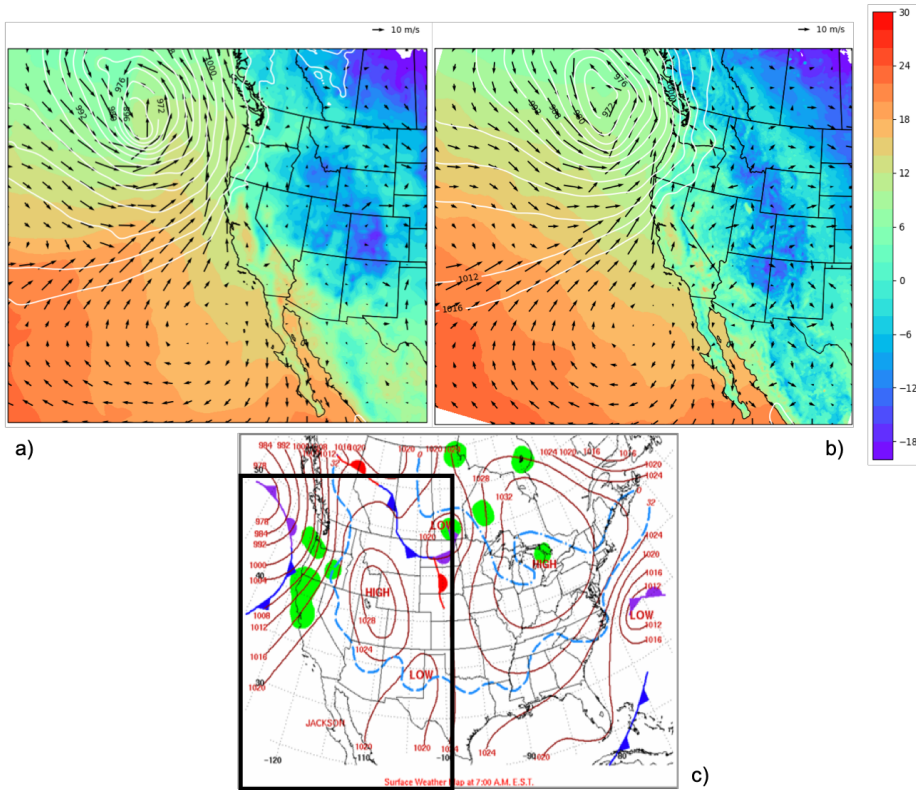
[9]



Deleted:

Formatted: Right: 0.63 cm

[10]



589

590 **Figure 4:** Mean sea level pressure (mslp) (white contour lines), surface temperature  
 591 (color shading) and 100-m wind direction (black arrows) at 7:00 UTC, 16 Feb. 2004  
 592 of ERA5 reanalysis (a) and RegCM 12km (b) respectively. (c) NCEP-NOA Surface  
 593 Analysis of pressure and fronts. The black box in (c) bounded the area represented  
 594 in (a) and (b)

595 The intermediate resolution (12 km) domain (Figure 3a) covers a wide area  
 596 encompassing California and a large portion of the coastal Pacific Ocean, with 23 vertical

Deleted: black

Deleted: f

Deleted: 2

Formatted: Right: 0.63 cm

600 levels and a parameterization for deep convection based on the Kain–Fritsch scheme  
 601 (Kain, 2004). The ERA-Interim driven simulation is initialized at 0000 UTC, 15 February  
 602 2004 (Table 2) and lasts until 0000 UTC 19 February 2004. This simulation drives a  
 603 corresponding RegCM4-NH run using a smaller domain centered over northern California  
 604 (Fig. 3a) at 3 km horizontal grid spacing and 41 vertical levels, with boundary conditions  
 605 updated at 6 hour intervals. In RegCM4-NH only the shallow convection component of  
 606 the Tiedtke scheme (Tiedtke, 1996) is activated. Simulated precipitation is compared with  
 607 the CHIRPS, CMORPH, TRMM, PRISM, NCEP/CPC observations described in Table 3.  
 608 First, we notice that the synoptic conditions characteristic of this case study, which are  
 609 fed into the RegCM4-NH model, are well reproduced by RegCM4 at 12 km, as shown in  
 610 Figure 4, where we compare the mean sea level pressure (mslp), surface temperature  
 611 and wind direction on 14 Feb at 7:00 am, as simulated by RegCM at 12 km (Fig.3b) with  
 612 corresponding fields from the ERA5 reanalysis (Fig.4a). The surface analysis of pressure  
 613 and fronts, derived from the operational weather maps prepared at the National Centers  
 614 for Environmental Prediction, Hydrometeorological Prediction Center, National Weather  
 615 Service ([https://www.wpc.ncep.noaa.gov/dailywxmap/index\\_20040216.html](https://www.wpc.ncep.noaa.gov/dailywxmap/index_20040216.html)) is also  
 616 reported in Figure 4c.  
 617 The observed precipitation datasets show similar patterns for the total accumulated  
 618 precipitation (Figure 5), in particular CHIRPS, PRISM and NCEP exhibit similar spatial  
 619 details and magnitudes of extremes. CHIRPS places a maximum around 42°N which is  
 620 not found in the other datasets. CMORPH and TRMM show lower precipitation maxima  
 621 and lesser spatial details due to their lower resolution, indicating that the performance of  
 622 satellite-based products may be insufficient as a stand alone product to validate the model  
 623 for this case.

Deleted: .

Deleted: 1

Deleted: 2

Deleted: 1

Deleted: used

Deleted:

Deleted: ( ) against rainfall data from the TRMM (0.25°x0.25°) (Huffman et al, 2007) dataset over the sea, and the CHIRPS (0.05°x0.05°) (Funk et al, 2015) dataset over the land

Deleted: .

Deleted: simulated

Deleted:

Deleted:

Deleted: ,

Deleted: the same variables inby

Deleted: 3

Deleted: ; finallyand t

Deleted:

Deleted: ,

Deleted: given

Deleted: (

Deleted: .

Deleted: 3

Deleted: )

Deleted: ing

Formatted: Right: 0.63 cm

651 In general, the observed precipitation datasets place the highest maxima on the terrain  
652 peaks, with extreme rainfall greater than 250 mm in 60 hours over the coastal mountains  
653 and greater than 100 – 175 mm elsewhere, (Fig. 5a). The black box in Fig 5 shows the  
654 area of the Russian River watershed, highlighting the locations of the observing systems,  
655 including Cazadero (CZD) and Bodega Bay (BBY) where the largest rainfall rates were  
656 detected, 269 mm and 124 mm in 60-h accumulated rainfall between 0000 UTC 16  
657 February and 1200 UTC 18 February 2004, respectively (Ralph et al., 2006).

658 The convection-permitting simulation captures the basic features of the observed  
659 precipitation, as shown for example in Fig.5, both in terms of spatial distribution and  
660 temporal evolution of rainfall (Fig.6a). However, it shows higher precipitation rates than  
661 observed over the sea and over the mountain chains, with lower intensities than observed  
662 in the south-east part of the mountain chain (Fig.5). By contrast, the 12-km simulation  
663 severely underestimates the magnitude of the precipitation event (Fig.5).

664 Concerning the timing and intensity of the event in the CZD subregion, 6-hourly  
665 accumulated precipitation (Fig.6a) averaged over the black box of Figure 5, shows that  
666 both the 3 km and 12 km simulations capture the onset of the event, but the peak intensity  
667 is strongly underestimated by the 12 km run, while it is well simulated by the 3 km run,  
668 although the secondary maximum is overestimated. Therefore, our results demonstrate  
669 that only the high resolution convection-permitting model captures this extreme event,  
670 and that parameterized convection has severe limits in this regard (Done et al. 2004; Lean  
671 et al. 2008; Weisman et al. 2008; Weusthoff et al. 2010; Schwartz 2014; Clark et al. 2016).

672

Deleted: The

Deleted: elevation

Deleted: of

Deleted: in the domain

Deleted: 4

Deleted: 4

Deleted: .4a

Deleted: respectively

Deleted:

Deleted: (Fig.4a)

Deleted: 4

Deleted: g and 5a

Deleted: 5

Deleted: 4

Deleted: g

Deleted: 4

Deleted: d

Deleted: 5

Deleted: red

Deleted: 4

Deleted: a

Deleted: overall,

Deleted: show

Deleted:

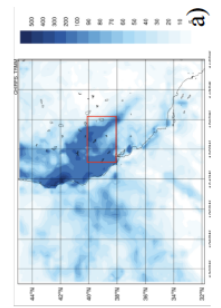
Deleted: ese

Deleted: s

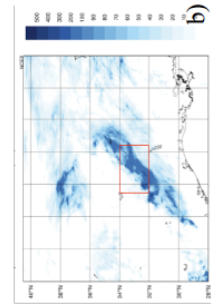
Formatted: Right: 0.63 cm

Total accumulated precipitation during the events (mm)

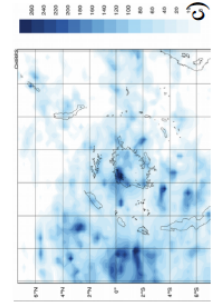
CAL



TEX



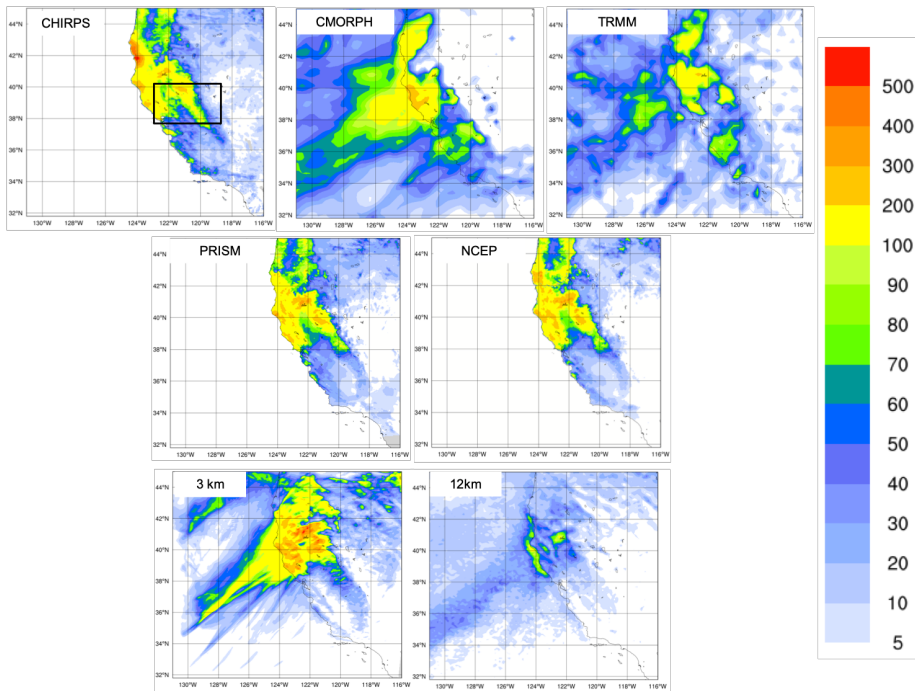
LKV



OBS 1

Deleted:

Formatted: Right: 0.63 cm



702

703 Figure 5. : Total accumulated precipitation (mm) during the California case:  
 704 CHIRPS, CMORPH, TRMM observations (top line), PRISM and NCEP Reanalysis  
 705 (middle line) and convection-permitting simulation with RegCM4-NH at 3km and  
 706 RegCM4 at 12km (bottom line) .The black box denotes the area where the spatial  
 707 average of 6-hourly accumulated precipitation is calculated and reported in Fig. 6.

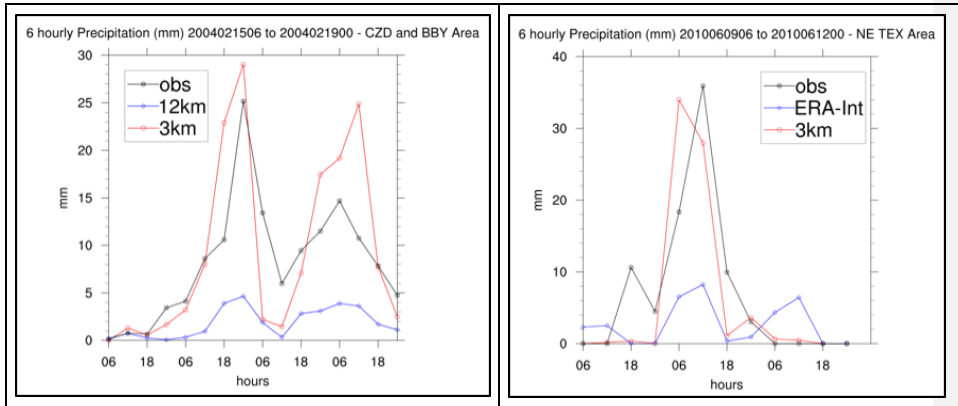
708

Deleted: 4

Deleted: 5

CAL (a)	TEX (b)
---------	---------

Formatted: Right: 0.63 cm



711 **Figure 6:** Time series of the 6 hourly accumulated precipitation (in mm on the y-  
 712 axis) during the CAL event (a) and during the TEX event (b). The blue lines show  
 713 RegCM4 12 Km and ERA interim 6 hourly accumulated precipitation averaged over  
 714 the areas indicated by the red square in Figure 3 (a,b) while the red line shows the  
 715 6 hourly accumulated precipitation simulated by RegCM4-NH. The observations are  
 716 shown with a black line.

Deleted: 5

Deleted: .

Deleted: 3 km

Deleted: in

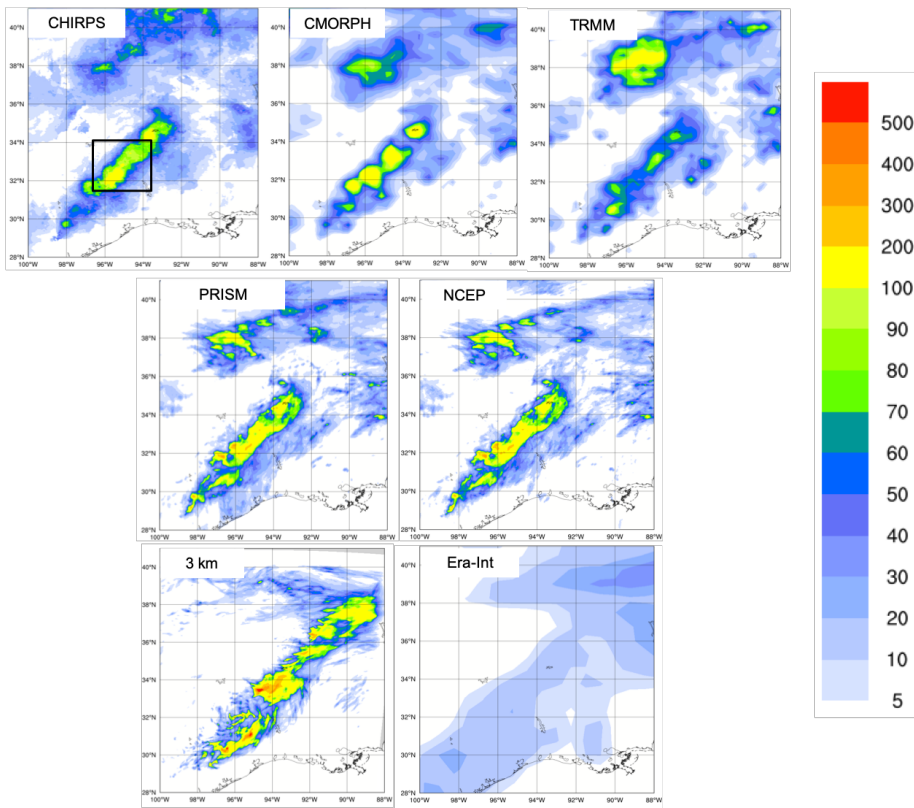
718 **Texas**

719 Case 2, hereafter referred to as TEX (Table 2), is a convective precipitation episode  
 720 exhibiting characteristics of the “Maya Express” flood events, linking tropical moisture  
 721 plumes from the Caribbean and Gulf of Mexico to midlatitude flooding over the central  
 722 United States (Higgins 2011). During the TEX event, an upper-level cutoff low over  
 723 northeastern Texas, embedded within a synoptic-scale ridge, moved slowly  
 724 northeastward. Strong low-level flow and moisture transport from the western Gulf of  
 725 Mexico progressed northward across eastern Texas. The event was characterized by  
 726 low-level moisture convergence, weak upper-level flow, weak vertical wind shear, and

Deleted: 1

Formatted: Right: 0.63 cm

732 relatively cold air (center of cutoff low), which favored the slow-moving convective storms  
 733 and nearly stationary thunderstorm outflow boundaries. The main flooding event in  
 734 eastern Texas occurred on June 10, 2010, with a daily maximum rainfall of 216.4 mm of  
 735 the region in the **black** box of Figure 7. (Higgins 2011).



Deleted: red  
 Deleted: grid  
 Deleted: 6  
 Deleted: 4b

736  
 737 **Figure 7: Total accumulated precipitation (mm) during the Texas case: CHIRPS,**  
 738 **CMORPH, TRMM observations (top line), PRISM and NCEP Reanalysis (central**  
 739 **line) and convection-permitting simulation with RegCM4-NH at 3 km grid spacing**  
 740 **and Era-Int (bottom line).The black box shows the area where the spatial average**  
 741 **of 6-hourly accumulated precipitation was calculated and reported in Figure 6.**

Deleted: 6

Deleted: .5

Formatted: Right: 0.63 cm



748  
749  
750  
751  
752  
753  
754  
755  
756  
757  
758  
759  
760  
761  
762  
763  
764  
765  
766  
767  
768  
769  
770

As for the California case, the observed precipitation datasets show coherent patterns for the total accumulated precipitation (Fig. 6), with the highest values related to the mesoscale convective system in eastern Texas (~ 200 mm), and another smaller area of high precipitation more to the north, approximately over Oklahoma. PRISM and NCEP capture similar spatial details and magnitudes of extremes, CHIRPS has lower precipitation extremes in the north compared to the other datasets, while CMORPH and TRMM show the lowest precipitation extremes and reduced spatial details as already noted for the California case.

The bottom panels in Figure 7 present precipitation as produced by the RegCM4-NH and the ERA-Interim reanalysis (driving data), respectively. ERA-Interim reproduces some of the observed features of precipitation, but with a substantial underestimation over the areas of maximum precipitation because of its coarse resolution. By comparison, the RegCM4-NH simulation (Fig. 7) shows an improvement in both pattern and intensity of precipitation, and is substantially closer to observations over eastern Texas. However, the precipitation area is slightly overestimated and the model is not capable of reproducing the small region of maximum precipitation in the north.

The time series of precipitation over eastern Texas from 9 to 12 June 2010 for observations (black line), ERA-Interim (blue line) and RegCM4-NH (red line) are reported in Figure 6b. Precipitation increases over this region from 00:00, 10 June, until it reaches

- Deleted: similar
- Deleted: . In general the precipitation observations show (Fig. 6) ...
- Deleted: with
- Deleted: maximum
- Deleted: amounts
- Deleted: detects
- Deleted: s
- Deleted: .
- Deleted: l
- Deleted: dataset
- Deleted: r
- Deleted: less
- Deleted: in general
- Deleted: we
- Deleted: In the daily precipitation observations for 10 [11]
- Deleted: Figures
- Deleted: 6
- Deleted: 4e and 4h
- Deleted: show
- Deleted: s
- Deleted: reproduced
- Deleted: the same information as in Figure 4b (bottom [12]
- Deleted: Era
- Deleted: and the RegCM4-NH
- Deleted: The
- Deleted: shows
- Deleted: n expected
- Deleted: it also shows a
- Deleted: pronounced
- Deleted: , given its coarser resolution,
- Deleted: s
- Deleted: 4h
- Deleted: are
- Deleted: in the non-hydrostatic simulation
- Deleted: (Figure 5b)
- Deleted: shown
- Deleted: F
- Deleted: .
- Deleted: 5
- Formatted: Right: 0.63 cm

819 the observed maximum at 12:00, 10 June (~35 mm), gradually decreasing afterwards  
820 until 6:00, 11 June. The RegCM4-NH simulation shows a more realistic temporal  
821 evolution than the ERA-Interim, which exhibits an overall underestimation [of precipitation](#).  
822 In general, the non-hydrostatic model produces precipitation values close to the  
823 observations, however, the simulated maximum is reached 6 hours earlier than observed.

824  
825

### 826 **Lake Victoria**

827 Case 3 focuses on Lake Victoria (LKV), with the purpose of testing RegCM4-NH on a  
828 complex and challenging region in terms of convective rainfall. It is estimated that each  
829 year 3,000-5,000 fishermen perish on the lake due to nightly storms (Red Cross, 2014).

830 In the Lake Victoria basin, the diurnal cycle of convection is strongly influenced by  
831 lake/land breezes driven by the thermal gradient between the lake surface and the  
832 surrounding land. As the land warms during the course of the day, a lake breeze is  
833 generated which flows from the relatively cooler water towards the warmer land surface.

834 The circulation is effectively reversed at night, when the land surface becomes cooler  
835 than the lake surface, leading to convergence over the lake and associated thermal  
836 instability.

837 In the LKV region, prevailing winds are generally easterly most of the year with some  
838 variability due to the movement of the ITCZ. The local diurnal circulation created by the  
839 presence of the lake within the larger scale easterly wind field creates two diurnal rainfall  
840 maxima. During daylight hours, when the lake breeze begins to advance inland,  
841 convergence is maximized on the eastern coast of the lake as the lake breeze interacts  
842 with the prevailing easterlies. Studies have also noted the importance of downslope

Formatted: Right: 0.63 cm

843 katabatic winds along the mountains to the east of the lake in facilitating convergence  
844 along the eastern coastal regions (Anyah et al. 2006). This creates a maximum in rainfall  
845 and convection on the eastern coast of LKV. Conversely, during nighttime hours, when  
846 the local lake circulation switches to flow from the land towards the lake, the prevailing  
847 easterlies create locally strong easterly flow across the lake and an associated maximum  
848 in convergence and rainfall on the western side of LKV.

849 The LKV simulation starts on 25 November 1999 and extends to the beginning of  
850 December 1999 (Table 2), covering a 5-day period which falls within the short-rain season  
851 of East Africa. The choice of 1999, an ENSO neutral year, was made in order to focus the  
852 analysis on local effects, such as the diurnal convection cycle in response to the lake/land  
853 breeze, with no influence of anomalous large scale conditions. A 1-dimensional lake  
854 model (Hostetler et al. 1993; Bennington et al. 2014) interactively coupled to RegCM4-  
855 NH was utilized to calculate the lake surface temperature (LST), since lake-atmosphere  
856 coupling has been shown to be important for the LKV (Sun et al. 2015; Song et al. 2004).  
857 This coupled lake model has been already used for other lakes, including Lake Malawi in  
858 southern Africa (Diallo et al. 2018). As with the other experiments, the boundary  
859 conditions are provided by a corresponding 12 km RegCM4 simulation employing the  
860 convection scheme of Tiedtke (1996).

861 At the beginning of the simulation, the LST over the lake is uniformly set to 26C, and is  
862 then allowed to evolve according to the lake-atmosphere coupling. [This initial LST value](#)  
863 [is based on previous studies. For example, Talling \(1969\) finds Lake Victoria surface](#)  
864 [temperatures ranging from 24.5-26°C during the course of the year. Several studies have](#)  
865 [used RCMs to investigate the Lake Victoria climate](#) (Anyah et al., 2006; Anyah and

Deleted: 1

Formatted: Right: 0.63 cm

867 [Semazzi 2009, Sun et al. 2015](#)), and found a significant relationship between lake  
 868 [temperature and rainfall depending on season. The value of 26°C is typical of the winter](#)  
 869 [season and was chosen based on preliminary sensitivity tests using different values of](#)  
 870 [initial temperature ranging from 24°C to 26°C.](#)

871 The synoptic feature favorable for the production of precipitation over the LKV in this  
 872 period corresponds to a large area of southeasterly flow from the Indian Ocean (Fig. [8a](#)),  
 873 [which](#), brings low-level warm moist air, into the LKV region facilitating the production of  
 874 convective instability and precipitation. This synoptic [situation](#), with a low-level  
 875 southeasterly jet off the Indian Ocean, is a common feature associated with high  
 876 precipitation, in the [area](#) (Anyah et al. 2006) is found in ERA5 (Figure [7a](#)).

877

a)	b)
----	----

Deleted: is initial LST value was chosen based on preliminary simulations and was shown to produce the most realistic precipitation for the period compared with CMORPH (Joyce et al, 2004)

Deleted: 7

Deleted: 6

Deleted: . This southeasterly flow

Deleted:

Deleted: es

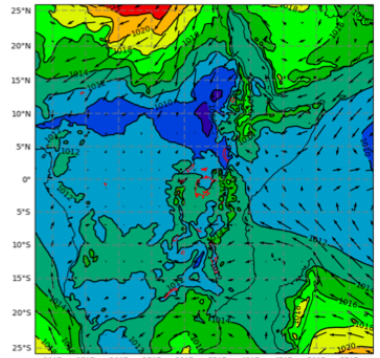
Deleted: etup

Deleted:

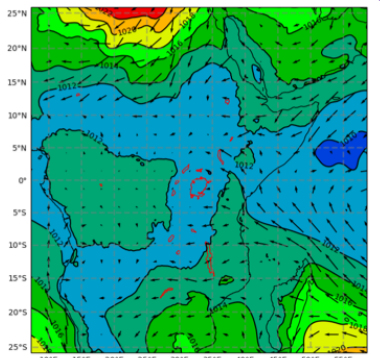
Deleted: production

Deleted: LKV region

Deleted: 6

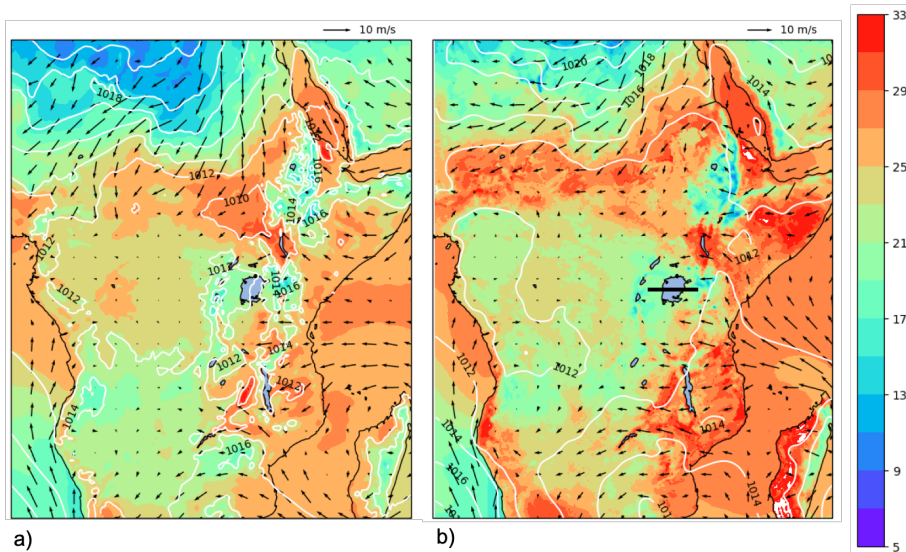


Deleted:



Deleted:

Formatted: Right: 0.63 cm



894

895

896

897

898

899

900

901

902

903

904

905

**Figure 8:** Mean sea level pressure (mslp) (white black contour lines), surface temperature (color shading) and 100-m wind direction (black arrows) averaged over the period 25 November 00:00 - 1 December 00:00, of ERA5 reanalysis (a) and RegCM 12km (b). The black line (b) shows the cross-section position represented in Fig. 9

The LKV region dynamics are quite distinct between nighttime and daytime and the rainfall in and around the lake has a pronounced diurnal cycle. To understand this strong diurnal cycle, Figure 9 shows a cross-section through the lake (32E to 34E, black line in right panel of Fig. 8) along 1S latitude at a period during strong nighttime (Fig. 9b,d; 6Z 30 November) and daytime convection (Fig. 9a,c; 12Z 29 November). During the day,

- Deleted: 7
- Deleted: 6
- Deleted: m
- Deleted: mean sea level pressure (mslp) (color shading) and 100-m wind direction (black arrows)
- Deleted: averaged over the period
- Deleted: 9
- Deleted: 2
- Deleted: The Victoria Lake and the others lakes in the domain are highlighted in red line
- Formatted: Font: 12 pt
- Deleted: 8
- Deleted: 7
- Deleted: o
- Deleted: o
- Deleted: bottom
- Deleted: 9
- Deleted: o
- Deleted: convection
- Deleted: 8
- Deleted: 7
- Deleted: a
- Deleted: 4
- Deleted: during strong
- Deleted: 8
- Deleted: 7
- Deleted: b
- Deleted: 3
- Formatted: Right: 0.63 cm

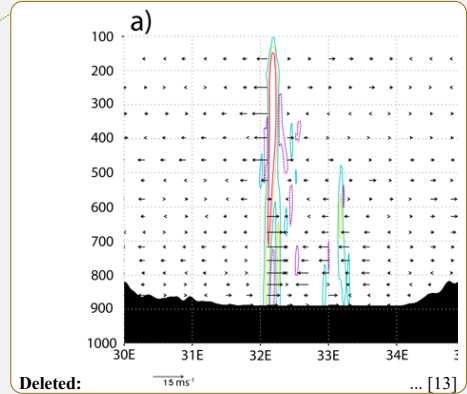
933 surface heating around the lake leads to a temperature differential between the land and  
 934 lake sufficient to generate a lake breeze, which causes divergence over the lake, while  
 935 over the surrounding highlands the environment is more conducive to convection (9a,c).  
 936 Conversely, during the night, a land breeze circulation is generated, which induces  
 937 convergence and convection over the lake (Figure 9b,d).

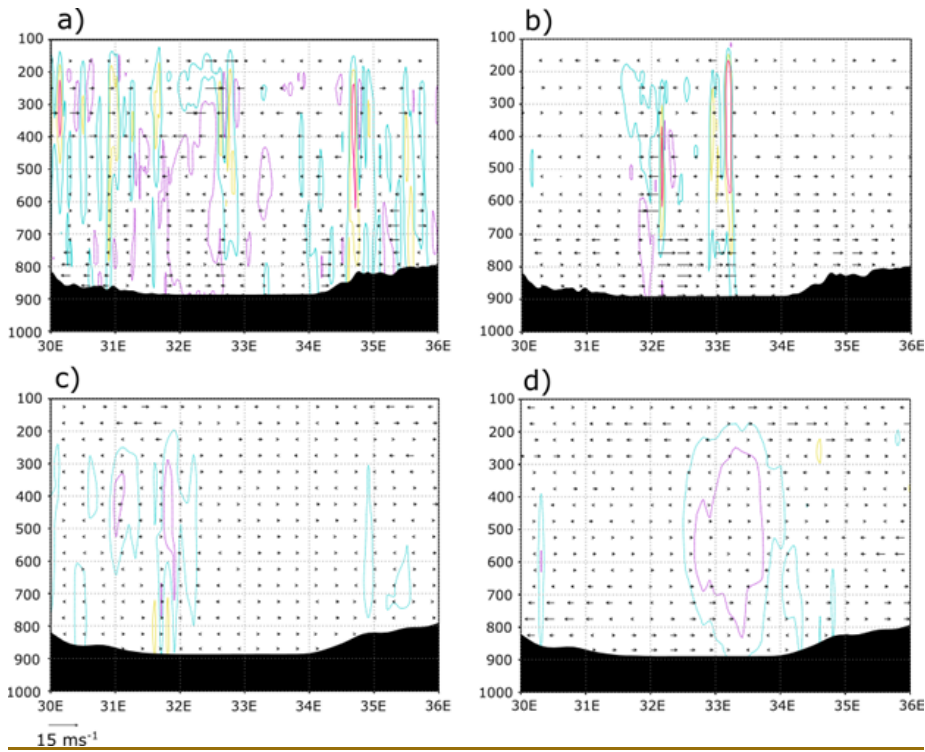
938 Comparing the 3 km simulation to the 12 km forcing run, we find that the localized  
 939 circulations created by local forcings (i.e. convection) are much stronger in the high  
 940 resolution experiment. We also find stronger and more localized areas of convective  
 941 updrafts as seen in the vertical velocities (9a,b) compared to the 12 km simulation (8c,d;  
 942 omega is shown instead of vertical velocity here because of the difference in model  
 943 output). The stronger convection simulated in the 3 km experiment is also tied to the  
 944 stronger temperature gradients between lake and land and between day and night (Figure  
 945 10).

946 This demonstrates that the 3km simulation is better equipped to simulate the localized  
 947 circulations associated with this complex land-lake system.

948

- Deleted: create
- Deleted: . This lake breeze promotes
- Deleted: 8
- Deleted: 7
- Deleted: is in opposition to the large scale easterly flow over the region and consequently strong convergence and convection is maximized in the highlands to the east of the lake (Fig.
- Deleted: the lake becomes the focus of
- Deleted: and consequently a focus for
- Deleted: as seen in
- Deleted: 8
- Deleted: 7
- Deleted: a
- Deleted: simulation
- Deleted: 3km simulation
- Deleted: 8
- Deleted: 7
- Deleted: 7
- Deleted: st
- Deleted: /
- Deleted: /
- Deleted: represented in the 3km simulation compared to than in the 12 km one, as shown in
- Deleted: f
- Deleted: 9
- Deleted: 8
- Deleted: by the Longitude-time (hourly) Hovmöller diagram of LKV domain surface temperature.





987

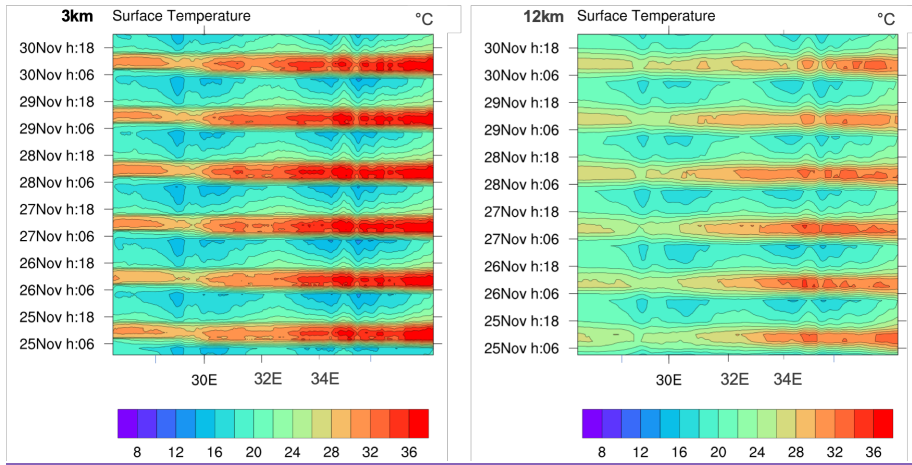
988 **Figure 9. Cross-section through 1S (red line in bottom right panel of Fig. 9) of the**  
 989 **mean (0-2N) zonal-wind anomaly (30E-36E) vectors and contoured vertical velocity**  
 990 **(m/s) at a) 12Z 29 November and b) 6Z 30 November from the 3km simulation.**  
 991 **Purple dashed contours indicate -0.1 m/s, light blue contours indicate 0.1 m/s,**  
 992 **yellow contours indicate 0.3 m/s, and red contours indicate 0.5 m/s. Lake Victoria**  
 993 **encompasses about 32E to 34E. The bottom 2 panels show the cross-section also**  
 994 **through 1S and mean zonal-wind anomaly vectors as in a) and b) but from the 12km**  
 995 **simulation at c) 12Z 29 November and d) 6Z 30 November. Purple dashed contours**

Deleted: 8

Deleted: 7

Formatted: Right: 0.63 cm

998 indicate -0.01 hPa/s, light blue dashed contours indicate -0.005 hPa/s, and yellow  
999 dashed contours indicate 0.005 hPa/s.



1000

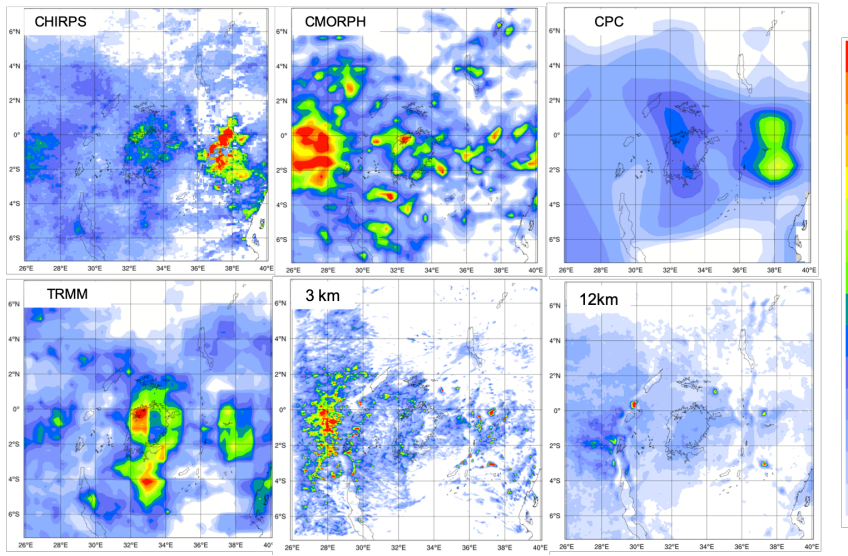
1001 Figure 10 : Longitude-time (hourly) Hovmöller diagram of LKV domain surface  
1002 temperature (shading, in °C). Panels correspond to the 3km simulation (left) and  
1003 12km simulation (right). The lake Victoria is between 32E and 34E longitude

Deleted: 9

Deleted: 8

Formatted: Right: 0.63 cm





1006

1007

1008

1009

Figure 11: Total accumulated precipitation during the LKV case measured by CHIRPS (top left), CMORPH (top center), CPC (top right) TRMM (bottom left) and calculated by RegCM4 at 3 km (bottom center) and 12 km (bottom right) .

1010

1011

1012

1013

1014

1015

1016

1017

1018

1019

Figure 11, finally reports, the total accumulated precipitation observed and simulated for the LKV case. TRMM and CPC show a similar pattern, with two-rainfall maxima of different intensities over the southeastern and northwestern lake areas. CMORPH shows a western rainfall maximum similar to TRMM and one large rainfall area almost entirely centered over the highlands to the west of the lake. Conversely in CHIRPS, a maximum is found to the east of the lake while several localized maxima occur over the lake. The differences between the observed datasets highlight the issue of observational uncertainty and the need to take into consideration shortcomings associated with the types of observational datasets considered. Different datasets can have significantly

Deleted: 9

Deleted: 0

Deleted: 9

Deleted: 4c

Deleted: shows

Deleted: measured

Deleted: for the total accumulated precipitation

Deleted: and the northwestern lake

Deleted: -area rainfall concentration, which is

Deleted: shows

Deleted: over the lake

Deleted: tself

Deleted: are seen

Formatted: Right: 0.63 cm

1033 different climatology, especially in areas of low data availability. For example, Prein and  
1034 Gobiet (2017) analyzed two gauge-based European-wide datasets, and seven global low-  
1035 resolution datasets, and found large differences across the observation products, often  
1036 of similar magnitude as the difference between model simulations. In this case and for  
1037 this area the observation uncertainty plays a big role especially at high resolution, and  
1038 highlights the need for an adequate observational network for model validation.

1039 However, even taking into account the elevated uncertainty existing in the observations  
1040 datasets, we find a significant underestimation of rain amounts in the 12 km run (Fig 11),  
1041 with a wide area of rainfall around 80mm over the whole of LKV. In contrast, the 3 km  
1042 simulation shows substantially greater detail, with rainfall patterns more in agreement with  
1043 the CMORPH observations. In particular, the 3 km simulation reproduces well the local  
1044 rainfall maxima on the western side of the lake, although these appear more localized  
1045 and with a multi-cell structure compared to CMORPH and TRMM. Additionally, the 12  
1046 km simulation underestimates the observed heavy rainfall totals in the highlands to the  
1047 west of the lake region, which are instead reproduced by the 3 km simulation.

1048 This last test case demonstrates the ability of RegCM4-NH in simulating realistic  
1049 convective activity over a morphologically complex region, which is a significant  
1050 improvement compared to the hydrostatic-coarse resolution model configuration.

## 1052 Conclusions and future outlook

1053 In this paper we have described the development of RegCM4-NH, a non hydrostatic  
1054 version of the regional model system RegCM4, which was completed in response to the  
1055

- Deleted: variability between
- Deleted: demonstrating that the spread of observation datasets from different sources are often compar
- Deleted: such
- Deleted: s
- Deleted: essential
- Formatted: Font:
- Formatted: Font: Highlight
- Deleted: shows that the total observed rainfall for the period is characterized by diurnal rainfall maxima associated with the local lake circulation. In particular, the north-western side of the lake shows a rainfall maximum exceeding 250mm during the 5-day simulation, while most of the north-west portion of the lake shows over 150mm in total rainfall. In addition, a weaker but still significant rainfall maximum is seen on the inland south-eastern coast of LKV.
- Deleted: for this case
- Deleted: , cComparing the 12 km simulated rainfall (Fig 11)
- Deleted: significantly
- Deleted: less
- Deleted: former
- Deleted: significantly more localization of the
- Deleted: which and this is
- Deleted: ed amount
- Deleted: otals
- Deleted: (observed in most dataset with different ... [15])
- Deleted: , which show the highest observed peak.
- Deleted: In particular, the 3 km simulation reproduces [16]
- Deleted: is unable to produce
- Deleted: with a strong underestimation
- Deleted: whereas these are well captured in
- Deleted: In summary, overall also Tt
- Deleted: that
- Deleted: the
- Deleted: robust
- Deleted: this
- Deleted: and that
- Deleted: is found
- Deleted: with respect
- Deleted: r
- Deleted: and hydrostatic
- Deleted: s
- Formatted: Right: 0.63 cm

1106 need of moving to simulations at convection-permitting resolutions of a few km. The  
1107 dynamical core of the non-hydrostatic version of MM5 has been thus incorporated into  
1108 the RegCM4 system, an approach facilitated by the fact that the this last is essentially an  
1109 evolution of the MM5. Some modifications to the MM5 dynamical core were also  
1110 implemented to increase the model stability for long term runs. RegCM4-NH also includes  
1111 two explicit cloud microphysics schemes needed to explicitly describe convection and  
1112 cloud processes in the absence of the use of cumulus convection schemes. Finally, we  
1113 presented a few case studies of explosive convection to illustrate how the model provides  
1114 realistic results in different settings and general improvements compared to the coarser  
1115 resolution hydrostatic version of RegCM4 for such types of events.

1116  
1117 As already mentioned, RegCM4-NH is currently being used for different projects, and  
1118 within these contests, is being run at grid spacings of a few km for continuous decadal  
1119 simulations, driven by reanalyses of observations or GCM boundary conditions (with the  
1120 use of an intermediate resolution domains) over different regions, such as the Alps, the  
1121 Eastern Mediterranean, Central-Eastern Europe and the Caribbeans. These projects,  
1122 involving multi-model intercomparisons, indicate that the performance of RegCM4-NH is  
1123 generally in line with that of other convection permitting models, and exhibits similar  
1124 improvements compared to coarser resolution models, such as a better simulation of the  
1125 precipitation diurnal cycle and of extremes at hourly to daily time scales. The results  
1126 obtained within the multi-model context confirm previous results from single-model  
1127 studies (Kendon et al. 2012, 2017, Ban et al. 2014, 2015; Prein et al. 2015, 2017), but  
1128 also strengthen the robustness of the findings through reduced uncertainty compared to  
1129 coarse resolution counterpart (Ban et al., 2021, Pichelli et al., 2021). The convection-  
1130 permitting scale can thus open the perspective of more robust projections of future  
1131 changes of precipitation, especially over short time scales.

1132  
1133  
1134 One of the problems of the RegCM4-NH dynamical core is that, especially for long runs  
1135 with varied meteorological conditions, a relatively short time step needs to be used for  
1136 stability reasons. This makes the model rather computationally demanding, although not

Deleted: Towards this goal we have incorporated into the RegCM4 framework Tt

Deleted: from

Deleted: RegCM system

Deleted: , as described in section 2

Deleted: RegCM4-NH is currently being used for different projects, such as the Flagship Pilot Study on convection permitting modeling (Coppola et al. 2020, Ban et al. 2021 , Pichelli et al. 2021) and the EU CP EU project (Hewitt and Lowe 2018). In these contexts, the model is being run at grid spacings of a few km for continuous decadal simulations, both driven by reanalyses of observations and GCM fields (in both cases with the use of an intermediate resolution run to act as interface) over different regions, such as the Alps, the Eastern Mediterranean, Central-Eastern Europe and the Caribbeans. This will help better validate and understand the model behavior at these high resolutions....

Formatted: Right: 0.63 cm

1156 more than other convection-permitting modeling systems such as the Weather Research  
1157 and Forecast model (WRF, Skamarok et al. 2008). For this reason, we are currently  
1158 incorporating within the RegCM system a very different and more computationally efficient  
1159 non-hydrostatic dynamical core, which will provide the basis for the next version of the  
1160 model, RegCM5, to be released in the future.

Deleted:

1161  
1162 Following the philosophy of the RegCM modeling system, RegCM4-NH is intended to be  
1163 a public, free, open source community resource for external model users. The non-  
1164 hydrostatic dynamical core has been implemented in a way that it can be activated in  
1165 place of the hydrostatic dynamics through a user-set switch, which makes the use of  
1166 RegCM4-NH particularly simple and flexible. We therefore envision that the model will be  
1167 increasingly used by a broad community so that a better understanding can be achieved  
1168 of its behavior, advantages and limitations.

Deleted: ,

Deleted: ,

1169

1170 **Code availability:** <https://zenodo.org/record/4603556>

1171 **Cases study configuration files:** <https://zenodo.org/record/5106399>

1172

1173

1174 **Author contribution:** CE prepared the manuscript with contributions from all co-authors  
1175 and coordinated research, SP, TA, GR carried out and analysed the simulations, PE  
1176 investigated solutions to stabilize/adapt the model at the km-scale and performed  
1177 preliminary validation tests, GG developed/adapted the model code, FDS contributed to  
1178 develop the coupled version of the model, NR developed one of the microphysics  
1179 scheme, GF supervised and coordinated all activities.

1180

1181 **Competing interests:** The authors declare that they have no conflict of interest.

1182

1183

## 1184 **References**

1185 Anyah, R., Semazzi, F. H. M., Xie, L., 2006: Simulated Physical Mechanisms Associated  
1186 with Climate Variability over Lake Victoria Basin in East Africa, Mon. Wea. Rev., 134  
1187 3588-3609.

1188

Formatted: Font: Bold

Formatted: Right: 0.63 cm

1192 Anthes, R. A., Hsie, E. -Y., & Kuo, Y. -H. (1987). Description of the Penn State/NCAR  
1193 Mesoscale Model: Version 4 (MM4) (No. NCAR/TN-282+STR). doi:10.5065/D64B2Z90  
1194  
1195 Anyah, R. O., F. H. M. Semazzi, L. Xie, 2006: Simulated Physical Mechanisms  
1196 Associated with Climate Variability over Lake Victoria Basin in East Africa. *Mon. Wea.*  
1197 *Rev.*, 134, 3588-3609,.  
1198  
1199 [Anyah RO, Semazzi F \(2009\) Idealized simulation of hydrodynamic characteristics of](#)  
1200 [Lake Victoria that potentially modulate regional climate. \*Int J Climatol\* 29\(7\):971–981.](#)  
1201 [doi:10.1002/joc.1795](#)  
1202  
1203 [Ashouri, Hamed, Kuo Lin Hsu, Soroosh Sorooshian, Dan K. Braithwaite, Kenneth R.](#)  
1204 [Knapp, L. Dewayne Cecil, Brian R. Nelson and Olivier P. Prat \(2015\). 'PERSIANN- CDR:](#)  
1205 [Daily precipitation climate data record from multisatellite observations for hydrological and](#)  
1206 [climate studies'. In: \*Bulletin of the American Meteorological Society\*. ISSN: 00030007.](#)  
1207 [DOI: 10.1175/BAMS-D-13-00068.1.](#)  
1208  
1209 Ban, N., J. Schmidli, and C. Schär, 2014: Evaluation of the convection-resolving regional  
1210 climate modeling approach in decade-long simulations. *J. Geophys. Res. Atmos.*, 119,  
1211 7889– 7907, <https://doi.org/10.1002/2014JD021478>.  
1212  
1213 Ban N, Schmidli J, Schär C (2015) Heavy precipitation in a changing climate: does short-  
1214 term summer precipitation increase faster? *Geophys Res Lett* 42:1165–1172.  
1215 <https://doi.org/10.1002/2014G L062588>  
1216 Ban, N., Caillaud, C., Coppola, E. *et al.* The first multi-model ensemble of regional climate  
1217 simulations at kilometer-scale resolution, part I: evaluation of precipitation. *Clim Dyn*  
1218 (2021). <https://doi.org/10.1007/s00382-021-05708-w>  
1219  
1220 Beheng, K.: A parameterization of warm cloud microphysical conversion processes,  
1221 *Atmos. Res.*, 33, 193–206, 1994

Formatted: Right: 0.63 cm

1222

1223 Bennington V, Notaro M, Holman KD, 2014: Improving Climate Sensitivity of Deep Lakes  
1224 within a Regional Climate Model and Its Impact on Simulated Climate, *J. Clim*, 27, 2886-  
1225 2911.

1226

1227 [Bretherton CS, McCaa JR, Grenier H \(2004\) A new parameterization for shallow cumulus](#)  
1228 [convection and its application to marine subtropical cloud-topped boundary layers. I.](#)  
1229 [Description and 1D results. \*Mon Weather Rev\* 132: 864– 882.](#)

1230

1231 Chan, S. C., E. J. Kendon, H. J. Fowler, S. Blenkinsop, N. M. Roberts, and C. A. T. Ferro,  
1232 2014: The value of high-resolution Met Office regional climate models in the simulation  
1233 of multi-hourly precipitation extremes. *J. Climate*, 27, 6155–6174,  
1234 <https://doi.org/10.1175/JCLI-D-13-00723.1>.

1235

1236 [Chen, Mingyue and Pingping Xie \(2008\). 'CPC Unified Gauge-based Analysis of Global](#)  
1237 [Daily Precipitation'. In: 2008 Western Pacific Geophysics Meeting. ISBN: 0026- 0576.](#)  
1238 [DOI: http://dx.doi.org/10.1016/S0026-0576\(07\)80022-5.](#)

1239

1240

1241 Clark, P., N. Roberts, H. Lean, S. P. Ballard, and C. Charlton-Perez, 2016: Convection-  
1242 permitting models: A step-change in rainfall forecasting. *Meteor. Appl.*, 23, 165–181,  
1243 <https://doi.org/10.1002/met.1538>.

1244

1245 [Coppola, E., Sobolowski, S., Pichelli, E. et al. A first-of-its-kind multi-model convection](#)  
1246 [permitting ensemble for investigating convective phenomena over Europe and the](#)  
1247 [Mediterranean. \*Clim Dyn\* 55, 3–34 \(2020\). <https://doi.org/10.1007/s00382-018-4521-8>](#)

1248

1249 [Coppola E, Giorgi F, Mariotti L, Bi X \(2012\) RegT-Band: a tropical band version of](#)  
1250 [RegCM4. \*Clim Res\* 52: 115–133](#)

1251

Deleted: ¶

Deleted: <https://doi.org/10.1175/JCLI-D-13-00723.1>

Formatted: Right: 0.63 cm

1254 Dacre, H. F., P. A. Clark, O. Martinez-Alvarado, M. A. Stringer, and D. A. Lavers, 2015:  
1255 How do atmospheric rivers form? Bull. Amer. Meteor. Soc., 96, 1243-1255,  
1256 <https://doi.org/10.1175/BAMS-D-14-00031>.

1257 Dale, M., A. Hosking, E. Gill, E. J. Kendon, H. J. Fowler, S. Blenkinsop, and S. C. Chan,  
1258 2018: Understanding how changing rainfall may impact on urban drainage systems; les-  
1259 sons from projects in the UK and USA. Water Pract. Technol., 13, 654–661,  
1260 <https://doi.org/10.2166/wpt.2018.069>.

1261

1262 Diallo, I., Giorgi, F. and Stordal, F. (2018) Influence of Lake Malawi on regional climate  
1263 from a double nested regional climate model experiment. Climate Dynamics, 50, 3397–  
1264 3411. <https://doi.org/10.1007/s00382-017-3811-x>

1265

1266 Dickinson, R.E., Errico, R.M., Giorgi, F. et al. A regional climate model for the western  
1267 United States. Climatic Change 15, 383–422 (1989). <https://doi.org/10.1007/BF00240465>

1268

1269 [Dickinson RE, Henderson-Sellers A, Kennedy P \(1993\) Bio -sphere– atmosphere transfer](#)  
1270 [scheme \(BATS\) version 1eas coupled to the NCAR community climate model. TechRep.](#)  
1271 [National Center for Atmospheric Research TechNote NCAR.TN-387+ STR, NCAR,](#)  
1272 [Boulder, CO](#)

1273

1274 Done, J., C. A. Davis, and M. L. Weisman, 2004: The next gener- ation of NWP: Explicit  
1275 forecasts of convection using the Weather Research and Forecasting (WRF) model.  
1276 Atmos. Sci. Lett., 5, 110–117, <https://doi.org/10.1002/asl.72>.

1277

1278 Dudhia, J., 1989: Numerical study of convection observed during the winter monsoon  
1279 experiment using a mesoscale two-dimensional model, J. Atmos. Sci., 46, 3077–3107.  
1280

1281 Durran D.R. and Klemp J.B.: A compressible model for the simulation of moist mountain  
1282 waves, Mon. Wea. Rev., 111, 2341–236, 1983.

1283

Deleted: <https://doi.org/10.1007/BF00240465>

Formatted: Right: 0.63 cm

1285 Elguindi N., Bi X., Giorgi F., Nagarajan, B. Pal J., Solmon F., Rauscher S., Zakey S.,  
1286 O'Brien T., Nogherotto R. and Giuliani G., 2017: Regional Climate Model  
1287 RegCMReference ManualVersion 4.7, 49 pp, <https://zenodo.org/record/4603616>

Deleted: <https://zenodo.org/record/4603616>

1288  
1289 [Emanuel KA \(1991\) A scheme for representing cumulus convection in large-scale](#)  
1290 [models. J Atmos Sci 48:2313–2335](#)

1291  
1292 [Fairall, C.W., E.F. Bradley, J.S. Godfrey, G.A. Wick, J.B. Edson, and G.S. Young, 1996a:](#)  
1293 [The cool skin and the warm layer in bulk flux calculations. J. Geophys. Res. 101, 1295-](#)  
1294 [1308.](#)

1295  
1296 [Fairall, C.W., E.F. Bradley, D.P. Rogers, J.B. Edson, G.S. Young, 1996b: Bulk](#)  
1297 [parameterization of air-sea fluxes for TOGA COARE. J. Geophys. Res. 101, 3747-3764.](#)

Formatted: Font: (Default) Arial, 12 pt

1298  
1299 Funk, C., Peterson, P., Landsfeld, M. et al. The climate hazards infrared precipitation with  
1300 stations—a new environmental record for monitoring extremes. Sci Data 2, 150066  
1301 (2015). <https://doi.org/10.1038/sdata.2015.66>

1302  
1303 Gimeno, L., R. Nieto, M. Vázquez, and D. A. Lavers, 2014: Atmospheric rivers: A mini-  
1304 review. Front. Earth Sci., 2, <https://doi.org/10.3389/feart.2014.00002>.

1305  
1306 Giorgi F (2019) Thirty years of regional climate modeling: where are we and where are  
1307 we going next? J Geophys Res Atmos 124:5696–5723

1308  
1309 [Giorgi F, Coppola E, Solmon F, Mariotti L and others \(2012\) RegCM4: model description](#)  
1310 [and preliminary tests over multiple CORDEX domains. Clim Res 52:7-29.](#)  
1311 <https://doi.org/10.3354/cr01018>

Deleted: Giorgi F et al (2012) RegCM4: model description and preliminary tests over multiple CORDEX domains. Clim Res 52:7–29

1312  
1313  
1314

Formatted: Right: 0.63 cm



1319 [Giorgi F, Francisco R, Pal JS \(2003\) Effects of a sub-gridscale topography and landuse](#)  
1320 [scheme on surface climateand hydrology. I. Effects of temperature and water](#)  
1321 [vapordisaggregation. J Hydrometeorol 4: 317– 333](#)  
1322  
1323 Giorgi F, Jones C, Asrar G (2009) Addressing climate information needs at the regional  
1324 level: the CORDEX framework. WMO Bull 175–183  
1325  
1326 Giorgi F, Mearns LO (1999) Introduction to special section: regional climate modeling  
1327 revisited. J Geophys Res 104:6335–6352  
1328  
1329 [Giorgi F, Marinucci MR, Bates G \(1993a\) Development of a second generation regional](#)  
1330 [climate model \(RegCM2\). I. Boundary layer and radiative transfer processes.](#)  
1331 [MonWeather Rev 121: 2794–2813](#)  
1332  
1333 Giorgi F, Marinucci MR, Bates G, DeCanio G (1993b) Development of a second  
1334 generation regional climate model (RegCM2), part II: convective processes and  
1335 assimilation of lateral boundary conditions. Mon Weather Rev 121:2814–2832  
1336  
1337 Giorgi, F., and G. T. Bates, 1989: The Climatological Skill of a Regional Model over  
1338 Complex Terrain. Mon. Wea. Rev., 117, 2325–2347, <https://doi.org/10.1175/1520->  
1339 [0493\(1989\)117<2325:TCSOAR>2.0.CO;2](https://doi.org/10.1175/1520-0493(1989)117<2325:TCSOAR>2.0.CO;2).  
1340 G. A. Grell, J. Dudhia and D. R. Stauffer, “A Description of the Fifth Generation Penn  
1341 State/NCAR Mesoscale Model (MM5),” NCAR Tech. Note, NCAR/TN-398+ STR,  
1342 Boulder, 1995, p. 122.  
1343  
1344 [Grell GA \(1993\) Prognostic evaluation of assumptions usedby cumulus](#)  
1345 [parameterizations. Mon Weather Rev 121: 764– 787](#)  
1346  
1347 [Grell, G., A.J. Dudhia, and D.R. Stauffer, 1994, A description of the fifth-generation Penn](#)  
1348 [State/NCAR mesoscale model \(MM5\). NCAR Technical Note, NCAR/TN- 398+STR.](#)  
1349

Formatted: Right: 0.63 cm

1350 Gunn, K. L. S., and J. S. Marshall, 1958: The distribution with size of aggregate  
1351 snowflakes. *J. Meteor.*, 15, 452–461, [https://doi.org/10.1175/1520-0469\(1958\)015<0452:TDWSOA>2.0.CO;2](https://doi.org/10.1175/1520-0469(1958)015<0452:TDWSOA>2.0.CO;2).

1353

1354 Gutowski Jr., W. J., Giorgi, F., Timbal, B., Frigon, A., Jacob, D., Kang, H.-S., Raghavan,  
1355 K., Lee, B., Lennard, C., Nikulin, G., O'Rourke, E., Rixen, M., Solman, S., Stephenson,  
1356 T., and Tangang, F.: WCRP COordinated Regional Downscaling EXperiment (CORDEX):  
1357 a diagnostic MIP for CMIP6, *Geosci. Model Dev.*, 9, 4087–4095,  
1358 <https://doi.org/10.5194/gmd-9-4087-2016>, 2016

1359

1360 [Holtslag A, de Bruijn E, Pan HL \(1990\) A high resolution air mass transformation model  
1361 for short-range weather fore-casting. \*Mon Weather Rev\* 118: 1561–1575](#)

1362

1363 [Hostetler SW, Bates GT, Giorgi F \(1993\) Interactive nesting of a lake thermal model within  
1364 a regional climate model for climate change studies. \*J Geophys Res\* 98: 5045– 5057](#)

1365

1366 Huffman, G. J., and Coauthors, 2007: The TRMM Multisatellite Precipitation Analysis  
1367 (TMPA): Quasi-global, multiyear, combined-sensor precipitation estimates at fine scales.  
1368 *J. Hydrometeorol.*, 8, 38–55, doi:<https://doi.org/10.1175/JHM560.1>

1369

1370 [Kiehl J, Hack J, Bonan G, Boville B, Breigleb B, WilliamsonD, Rasch P \(1996\)  
1371 Description of the NCAR Commun -ity Climate Model \(CCM3\). National Center for  
1372 Atmo spheric Research Tech Note NCAR/TN-420+ STR, NCAR,Boulder, CO](#)

1373

1374 Lean, H. W., P. A. Clark, M. Dixon, N. M. Roberts, A. Fitch, R. Forbes, and C. Halliwell,  
1375 2008: Characteristics of high- resolution versions of the Met Office Unified Model for  
1376 forecasting convection over the United Kingdom. *Mon. Wea. Rev.*, 136, 3408–3424,  
1377 <https://doi.org/10.1175/2008MWR2332.1>.

1378

Deleted: <https://doi.org/10.1175/JHM560.1>

Formatted: Right: 0.63 cm

1380 Lind, P., D. Lindstedt, E. Kjellstrom, and C. Jones, 2016: Spatial and temporal  
1381 characteristics of summer precipitation over central Europe in a suite of high-resolution  
1382 climate models. *J. Climate*, 29, 3501–3518, <https://doi.org/10.1175/JCLI-D-15-0463.1>.

1383

1384 Hewitt, C. D., and J. A. Lowe, 2018: Toward a European climate prediction system. *Bull.*  
1385 *Amer. Meteor. Soc.*, 99, 1997–2001, <https://doi.org/10.1175/BAMS-D-18-0022.1>.

1386 Hong, S.-Y., H.-M. H. Juang, and Q. Zhao, 1998: Implementation of prognostic cloud  
1387 scheme for a regional spectral model, *Mon. Wea. Rev.*, 126, 2621–2639.

1388

1389 Hong, S.-Y., J. Dudhia, and S.-H. Chen, 2004: A Revised Approach to Ice Microphysical  
1390 Processes for the Bulk Parameterization of Clouds and Precipitation, *Mon. Wea. Rev.*,  
1391 132, 103–120.

1392

1393 Hong, S.-Y., and J.-O. J. Lim, 2006: The WRF Single-Moment 6-Class Microphysics  
1394 Scheme (WSM6), *J. Korean Meteor. Soc.*, 42, 129–151

1395

1396 Hostetler SW, Bates GT, Giorgi F, 1993: Interactive Coupling of Lake Thermal Model with  
1397 a Regional climate Model, *J. Geophys. Res.*, 98(D3), 5045-5057.

1398

1399 [Huffman, George J., David T. Bolvin, Eric J. Nelkin, David B. Wolff, Robert F. Adler,](#)

1400 [Guojun Gu, Yang Hong, Kenneth P. Bowman and Erich F. Stocker \(2007\). The TRMM](#)

1401 [Multisatellite Precipitation Analysis \(TMPA\): Quasi-Global, Multiyear, Combined-Sensor](#)

1402 [Precipitation Estimates at Fine Scales. DOI: 10.1175/JHM560.1.](#)

1403

1404 Joyce, Robert J., John E. Janowiak, Phillip A. Arkin, Pingping Xie, 2004: CMORPH: A  
1405 Method that Produces Global Precipitation Estimates from Passive Microwave and  
1406 Infrared Data at High Spatial and Temporal Resolution. *J. Hydrometeor.*, 5, 487–503

1407

Formatted: Space Before: 12 pt, After: 12 pt

Formatted: Right: 0.63 cm

1408 Kain, J. S., 2004: The Kain–Fritsch convective parameterization: An update. *J. Appl.*  
1409 *Meteor.*, 43, 170–181, [https://doi.org/10.1175/1520-](https://doi.org/10.1175/1520-0450(2004)043)  
1410 [0450\(2004\)043](https://doi.org/10.1175/1520-0450(2004)043)<0170:TKCPAU>2.0.CO;2.

Deleted: [https://doi.org/10.1175/1520-0450\(2004\)043](https://doi.org/10.1175/1520-0450(2004)043)

1411  
1412 [Kain, J. S., and J. M. Fritsch, 1990: A one-dimensional entraining/ detraining plume model](#)  
1413 [and its application in convective parameterization, \*J. Atmos. Sci.\*, 47, 2784–2802.](#)

1414  
1415 Kendon, E. J., N. M. Roberts, C. A. Senior, and M. J. Roberts, 2012: Realism of rainfall  
1416 in a very high-resolution regional climate model. *J. Climate*, 25, 5791–5806,  
1417 [https://doi.org/ 10.1175/JCLI-D-11-00562.1](https://doi.org/10.1175/JCLI-D-11-00562.1).

1418  
1419 Kendon, E. J., and Coauthors, 2017: Do convection-permitting regional climate models  
1420 improve projections of future precipitation change? *Bull. Amer. Meteor. Soc.*, 98, 79–93,  
1421 [https://doi.org/ 10.1175/BAMS-D-15-0004.1](https://doi.org/10.1175/BAMS-D-15-0004.1)

1422  
1423 Kessler, E., 1969: On the Distribution and Continuity of Water Substance in Atmospheric  
1424 Circulations. *Meteor. Monogr.*, No. 32, Amer. Meteor. Soc., 84 pp.

1425  
1426 Khairoutdinov, M. and Kogan, Y.: A new cloud physics parameterization in a large-eddy  
1427 simulation model of marine stratocumulus, *B. Am. Meteorol. Soc.*, 128, 229–243, 2000

1428  
1429 Klemp, J.B. and Dudhia, J.: An Upper Gravity-Wave Absorbing Layer for NWP  
1430 Applications, *Monthly Weather Review*, 176, 3987-4004, 2008.

1431  
1432 Klemp, J. B. and D. K. Lilly: Numerical simulation of hydrostatic mountain waves, *J.*  
1433 *Atmos. Sci.*, 35, 78–107, 1978.

1434  
1435 Lin, Y., Farley, R., and Orville, H.: Bulk parameterization of the snow field in a cloud  
1436 model, *J. Appl. Meteor. Clim.*, 22, 1065–1092, 1983.

1437

Formatted: Right: 0.63 cm

1439 Marshall, J. S., and W. McK. Palmer, 1948: The distribution of raindrops with size. J.  
1440 Meteor., 5, 165–166.  
1441  
1442 [Matte, Dominic; Laprise, René; Thériault, Julie M.; Lucas-Picher, Philippe \(2017\). Spatial](#)  
1443 [spin-up of fine scales in a regional climate model simulation driven by low-resolution](#)  
1444 [boundary conditions. Climate Dynamics, 49\(1-2\), 563–574. doi:10.1007/s00382-016-](#)  
1445 [3358-2](#)

1446  
1447 [Mlawer, E. J., S. J. Taubman, P. D. Brown, M. J. Iacono, and S. A. Clough, 1997:](#)  
1448 [Radiative transfer for inhomogeneous atmospheres: RRTM, a validated correlated-k](#)  
1449 [model for the longwave. J. Geophys. Res., 102, 16,663-16,682](#)

1450  
1451 Nogherotto, R., Tompkins, A.M., Giuliani, G., Coppola, E. and Giorgi, F.: Numerical  
1452 framework and performance of the new multiple-phase cloud microphysics scheme in  
1453 RegCM4. 5: precipitation, cloud microphysics, and cloud radiative effects. Geoscientific  
1454 Model Development, 9(7), 2533-2547, 2016

1455  
1456 [Oleson, K. W., Lawrence, D. M., Bonan, G. B., Drewniak, B., Huang, M., Koven, C. D.,](#)  
1457 [Levis, S., Li, F., Riley, W. J., Subin, Z. M., Swenson, S. C., Thornton, P. E., Bozbiyik, A.,](#)  
1458 [Fisher, R., Kluzek, E., Lamarque, J. -F., Lawrence, P. J., Leung, L. R., Lipscomb, W.,](#)  
1459 [Muszala, S., Ricciuto, D. M., Sacks, W., Sun, Y., Tang, J., and Yang, Z. -L:Technical](#)  
1460 [Description of version 4.5 of the Community Land Model \(CLM\),Ncar Technical Note](#)  
1461 [NCAR/TN-503+STR, National Center for Atmospheric Research, Boulder, CO, 422 pp,](#)  
1462 [DOI: 10.5065/D6RR1W7M, 2013.](#)

1463  
1464 [Pal JS, Small E, Eltahir E \(2000\) Simulation of regional-scale water and energy budgets:](#)  
1465 [representation of subgrid cloud and precipitation processes within RegCM. J Geo-phys](#)  
1466 [Res 105: 29579–29594](#)

1467  
1468 Pal JS et al (2007) The ICTP RegCM3 and RegCNET: regional climate modeling for the  
1469 developing world. Bull Am Meteorol Soc 88:1395–1409

Formatted: Right: 0.63 cm

1470  
1471 Pichelli, E., Coppola, E., Sobolowski, S. *et al.* The first multi-model ensemble of regional  
1472 climate simulations at kilometer-scale resolution part 2: historical and future simulations  
1473 of precipitation. *Clim Dyn* (2021). <https://doi.org/10.1007/s00382-021-05657-4>  
1474  
1475 [Prein, Andreas F. and Andreas Gobiet \(2017\). 'Impacts of uncertainties in European](#)  
1476 [gridded precipitation observations on regional climate analysis'. In: International Journal](#)  
1477 [of Climatology. ISSN: 10970088. DOI: 10.1002/joc.4706](#)  
1478  
1479 Prein, A. F. et al. A review on regional convection-permitting climate modeling:  
1480 demonstrations, prospects, and challenges. *Rev. Geophys.* 53, 323–361 (2015).  
1481  
1482 Ralph, F. M., P. J. Neiman, G. A. Wick, S. I. Gutman, M. D. Dettinger, D. R. Cayan, and A.  
1483 B. White, 2006: Flooding on California's Russian River: Role of atmospheric rivers.  
1484 *Geophys. Res. Lett.*, 33, L13801, <https://doi.org/10.1029/2006GL026689>  
1485  
1486 Ralph, F. M., M. D. Dettinger, M. M. Cairns, T. J. Galarneau, and J. Eylander, 2018:  
1487 Defining "atmospheric river": How the Glossary of Meteorology helped resolve a debate.  
1488 *Bull. Amer. Meteor. Soc.*, 99, 837–839, <https://doi.org/10.1175/BAMS-D-17-0157.1>  
1489  
1490 Rutledge, S. A., and P. V. Hobbs, 1983: The mesoscale and microscale structure and  
1491 organization of clouds and precipitation in midlatitude cyclones. Part VIII: A model for the  
1492 "seeder-feeder" process in warm-frontal rainbands. *J. Atmos. Sci.*, 40, 1185–1206.  
1493  
1494 Skamarock WC, Klemp JB, Dudhia J, Gill DO, Barker DM, Duda MG, Huang XY, Wang  
1495 W, Powers JG. 2008. 'A description of the advanced research WRF version 3', Technical  
1496 Note NCAR/TN-475+STR. NCAR: Boulder, CO  
1497  
1498 Schwartz, C. S., 2014: Reproducing the September 2013 record-breaking rainfall over  
1499 the Colorado Front Range with high-resolution WRF forecasts. *Wea. Forecasting*, 29,  
1500 393–402, <https://doi.org/10.1175/WAF-D-13-00136.1>

Formatted: Right: 0.63 cm

1501  
1502 Sitz, L. E., F. Sante, R. Farneti, R. Fuentes-Franco, E. Coppola, L. Mariotti, M. Reale, et  
1503 al. 2017. "Description and Evaluation of the Earth System Regional Climate Model  
1504 (RegCM-ES)." Journal of Advances in Modeling Earth Systems.  
1505 doi:10.1002/2017MS000933  
1506  
1507 Song Y, Semazzi HMF, Xie L, Ogallo LJ, 2004: A coupled regional climate model for the  
1508 Lake Victoria Basin of East Africa. Int. J. Climatol. 24: 57-75.  
1509  
1510 Sun X, Xie L, Semazzi F, Liu B, 2015: Effect of Lake Surface Temperature on the Spatial  
1511 Distribution and Intensity of the Precipitation over the Lake Victoria Basin. Mon. Wea.  
1512 Rev. 143: 1179-1192.  
1513  
1514 Sundqvist, H., Berge, E., and Kristjansson, J.: Condensation and cloud parameterization  
1515 studies with a mesoscale numerical weather prediction model, Mon. Weather Rev., 117,  
1516 1641–1657, 1989.  
1517  
1518 [Talling, J. F. \(1969\) The incidence of vertical mixing, and some biological and chemical](#)  
1519 [consequences, in tropical African lakes, Verh. Int. Ver. Limnol. 17, 998-1012 DOI:](#)  
1520 [10.1080/03680770.1968.11895946](#)  
1521  
1522 [Tiedtke, M., 1989, A comprehensive mass flux scheme for cumulus parametrization in](#)  
1523 [large-scale models. Mon. Weather Rev., 117, 1779–1800](#)  
1524  
1525 Tiedtke, M., 1993: Representation of Clouds in Large-Scale Models. Mon. Wea. Rev.,  
1526 121, 3040–3061, [https://doi.org/10.1175/1520-0493\(1993\)121](https://doi.org/10.1175/1520-0493(1993)121<3040:ROCILS>2.0.CO;2)  
1527  
1528 Tiedtke, M., . 1996: An extension of cloud-radiation parameterization in the ECMWF  
1529 model: The representation of subgrid-scale variations of optical depth. Mon. Wea. Rev.,  
1530 124, 745–750  
1531

Formatted: Line spacing: Multiple 1.15 li

Formatted: Font: (Default) Arial, 12 pt

Formatted: Right: 0.63 cm

1532 Tompkins, A.: Ice supersaturation in the ECMWF integrated fore-cast system, Q. J. Roy.  
1533 Meteor. Soc., 133, 53–63, 2007  
1534  
1535 Tripoli, G. J., and W. R. Cotton, 1980: A numerical investigation of several factors  
1536 contributing to the observed variable intensity of deep convection over south Florida. J.  
1537 Appl. Meteor., 19, 1037–1063.  
1538  
1539 Williams PD. 2009. A proposed modification to the Robert–Asselin time filter. Mon.  
1540 Weather Rev. 137: 2538–2546  
1541  
1542 Weisman, M. L., C. Davis, W. Wang, K. W. Manning, and J. B. Klemp, 2008: Experiences  
1543 with 0–36-h explicit convective forecasts with the WRF-ARW model. Wea. Forecasting,  
1544 23, 407–437, <https://doi.org/10.1175/2007WAF2007005.1>  
1545  
1546 Weusthoff, T., F. Ament, M. Arpagaus, and M. W. Rotach, 2010: Assessing the benefits  
1547 of convection-permitting models by neighborhood verification: Examples from MAP D-  
1548 PHASE. Mon. Wea. Rev., 138, 3418–3433, <https://doi.org/10.1175/2010MWR3380.1>.  
1549  
1550 [Zeng X, Zhao M, Dickinson RE \(1998\) Intercomparison of bulk aerodynamic algorithms](#)  
1551 [for the computation of seasurface fluxes using TOGA COARE and TAO data. J Clim 11:](#)  
1552 [2628–2644](#)  
1553  
1554 Zhu, Y., and R. E. Newell, 1998: A proposed algorithm for moisture fluxes from  
1555 atmospheric rivers. Mon. Wea. Rev., 126, 725–735, [https://doi.org/10.1175/1520-0493\(1998\)126<0725:APAFMF>2.0.CO;2](https://doi.org/10.1175/1520-0493(1998)126<0725:APAFMF>2.0.CO;2).  
1556  
1557  
1558

Deleted: <https://doi.org/10.1175/2010MWR3380.1>

Formatted: Right: 0.63 cm



Page 2: [1] Deleted	Emanuela Pichelli	29/06/2021 14:02:00
Page 2: [1] Deleted	Emanuela Pichelli	29/06/2021 14:02:00
Page 2: [1] Deleted	Emanuela Pichelli	29/06/2021 14:02:00
Page 2: [1] Deleted	Emanuela Pichelli	29/06/2021 14:02:00
Page 2: [1] Deleted	Emanuela Pichelli	29/06/2021 14:02:00
Page 2: [1] Deleted	Emanuela Pichelli	29/06/2021 14:02:00
Page 2: [1] Deleted	Emanuela Pichelli	29/06/2021 14:02:00
Page 2: [1] Deleted	Emanuela Pichelli	29/06/2021 14:02:00
Page 2: [1] Deleted	Emanuela Pichelli	29/06/2021 14:02:00
Page 2: [1] Deleted	Emanuela Pichelli	29/06/2021 14:02:00
Page 2: [2] Deleted	FILIPPO GIORGI	21/07/2021 07:20:00
Page 2: [2] Deleted	FILIPPO GIORGI	21/07/2021 07:20:00
Page 2: [2] Deleted	FILIPPO GIORGI	21/07/2021 07:20:00
Page 2: [2] Deleted	FILIPPO GIORGI	21/07/2021 07:20:00
Page 2: [3] Deleted	FILIPPO GIORGI	21/07/2021 07:39:00
Page 2: [3] Deleted	FILIPPO GIORGI	21/07/2021 07:39:00
Page 2: [3] Deleted	FILIPPO GIORGI	21/07/2021 07:39:00
Page 2: [3] Deleted	FILIPPO GIORGI	21/07/2021 07:39:00

▼  
▲ Page 2: [3] Deleted FILIPPO GIORGI 21/07/2021 07:39:00

▼  
▲ Page 2: [3] Deleted FILIPPO GIORGI 21/07/2021 07:39:00

▼  
▲ Page 2: [3] Deleted FILIPPO GIORGI 21/07/2021 07:39:00

▼  
▲ Page 2: [4] Deleted FILIPPO GIORGI 21/07/2021 08:10:00

▼  
▲ Page 2: [4] Deleted FILIPPO GIORGI 21/07/2021 08:10:00

▼  
▲ Page 2: [4] Deleted FILIPPO GIORGI 21/07/2021 08:10:00

▼  
▲ Page 2: [4] Deleted FILIPPO GIORGI 21/07/2021 08:10:00

▼  
▲ Page 2: [4] Deleted FILIPPO GIORGI 21/07/2021 08:10:00

▼  
▲ Page 2: [4] Deleted FILIPPO GIORGI 21/07/2021 08:10:00

▼  
▲ Page 2: [4] Deleted FILIPPO GIORGI 21/07/2021 08:10:00

▼  
▲ Page 2: [4] Deleted FILIPPO GIORGI 21/07/2021 08:10:00

▼  
▲ Page 2: [4] Deleted FILIPPO GIORGI 21/07/2021 08:10:00

▼  
▲ Page 2: [4] Deleted FILIPPO GIORGI 21/07/2021 08:10:00

▼  
▲ Page 2: [4] Deleted FILIPPO GIORGI 21/07/2021 08:10:00

▼  
▲ Page 2: [4] Deleted FILIPPO GIORGI 21/07/2021 08:10:00

▼  
▲ Page 2: [5] Deleted FILIPPO GIORGI 21/07/2021 07:47:00

▼  
▲ Page 2: [5] Deleted FILIPPO GIORGI 21/07/2021 07:47:00

▼

▲	Page 2: [5] Deleted	FILIPPO GIORGI	21/07/2021 07:47:00
▼			
▲	Page 2: [6] Deleted	Emanuela Pichelli	29/06/2021 15:39:00
▼			
▲	Page 2: [6] Deleted	Emanuela Pichelli	29/06/2021 15:39:00
▼			
▲	Page 2: [7] Deleted	FILIPPO GIORGI	21/07/2021 07:48:00
▼			
▲	Page 2: [7] Deleted	FILIPPO GIORGI	21/07/2021 07:48:00
▼			
▲	Page 2: [7] Deleted	FILIPPO GIORGI	21/07/2021 07:48:00
▼			
▲	Page 17: [8] Deleted	Paolo Stocchi	05/07/2021 11:11:00
▼			
▲	Page 17: [9] Deleted	Paolo Stocchi	05/07/2021 11:11:00
▼			
▲	Page 17: [10] Deleted	Paolo Stocchi	05/07/2021 11:11:00
▼			
▲	Page 25: [11] Deleted	Paolo Stocchi	23/06/2021 12:47:00
▼			
▲	Page 25: [12] Deleted	Emanuela Pichelli	13/07/2021 17:45:00
▼			
▲	Page 30: [13] Deleted	Russell Glazer	24/06/2021 17:40:00
▼			
▲	Page 34: [14] Deleted	FILIPPO GIORGI	21/07/2021 11:50:00
▼			
▲	Page 34: [15] Deleted	FILIPPO GIORGI	21/07/2021 11:51:00
▼			
▲			

